CHEMISTRY
A EUROPEAN JOURNAL

DOI: 10.1002/chem.200801428

New 3π-2Spiro Ladder-Type Phenylene Materials: Synthesis, Physicochemical Properties and Applications in OLEDs

Nicolas Cocherel,[a] Cyril Poriel,*[a] Joëlle Rault-Berthelot,*[a] Frédéric Barrière,[a] Nathalie Audebrand,[a] Alexandra M. Z. Slawin,[b] and Laurence Vignau[c]

Abstract: New routes to ladder-type phenylene materials **1** and **2** are described. The oligomers **1** and **2**, which possess a "3π-2spiro" architecture, have been synthesized by using extended diketone derivatives **3** and **10** as key intermediates. The physicochemical properties of the new blue-light emitter **2** were studied in detail and compared with those of the less-extended **1**. Owing to the recent development of fluorenone derivatives and their corresponding more conjugated analogues as potential electron-transport materials in organic light-emitting diodes (OLEDs) and as n-type materials for photovoltaic applications, we also report herein the thermal, optical and electrochemical behavior of the key intermediates, diketones **3** and **10**. Finally, the application of dispiro **2** as a new light-emitting material in OLEDs is reported.

Keywords: ladder pentaphenylenes · luminescence · organic light-emitting diodes · semiconductors · spiro compounds

Introduction

Phenylene-based polymers are one of the most important classes of blue-emitting materials used in organic light-emitting diodes (OLEDs).[1] Three classes of polyphenylene that have been of particular interest are polyfluorenes, polyindenofluorenes and ladder-type poly-*p*-phenylene.[2,3] These polymers show blue to blue-green emission in solution. As the chain rigidity increases with an increasing number of fused planar rings, a bathochromic shift of the emission wavelength is observed, that is, 410 nm for polyfluorenes, 430 nm for polyindenofluorenes and 450 nm for ladder-type poly-*p*-phenylene. However, several groups have shown that, in the solid state, the emission is unstable due to the appearance of long-wavelength emission bands, which were assigned to excimer formation[4,5] and to ketone defects.[6,7] Among the numerous solutions that have been proposed to suppress this long-wavelength emission, the introduction of a rigid spiro linkage, such as spirobifluorene, into the polymer/oligomer backbone has been extensively developed. This spiro concept in electronics,[8,9] based on the connection, through an sp^3-hybridized carbon atom, of two molecular π systems (the 2π-1spiro concept, Figure 1) with equal or different functions (for example, emission, charge transport) has been widely studied by Tour[10–13] and Salbeck[14–19] and their co-workers. The use of such a linkage has been demonstrated to strongly enhance the OLED properties, that is, suppress excimer formation and ketonic defects, increase the thermal and morphological stability, enhance the quantum yield, improve the solubility and so forth.

For the last 20 years Müllen and Scherf and co-workers have designed many ladder-type oligomers and polymers for various optoelectronic applications, which has led to the significant enhancement in the performance of organic devices.[2,3,20–25] However, to the best of our knowledge, the synthesis of such oligomers incorporating spiro linkages has only been reported in a few papers.[26,27] In this context, we recently designed new blue luminescent dispiro building blocks, such as **1**, called dispirofluorene-indenofluorene

[a] N. Cocherel, Dr. C. Poriel, Dr. J. Rault-Berthelot, Dr. F. Barrière, Dr. N. Audebrand
Université de Rennes 1
UMR CNRS 6226 "Sciences Chimiques de Rennes"
Bat 10C, Campus de Beaulieu, 35042 Rennes Cedex (France)
Fax: (+33) 223-236732
E-mail: cyril.poriel@univ-rennes1.fr
joelle.rault-berthelot@univ-rennes1.fr

[b] Prof. Dr. A. M. Z. Slawin
School of Chemistry, University of St Andrews
North Haugh, St Andrews
Fife, KY16 9ST (UK)

[c] Dr. L. Vignau
Université de Bordeaux, IMS/UMR CNRS 5218-site
ENSCPB, 16 Avenue Pey-Berland, 33607 Pessac Cedex (France)

Supporting Information for this article is available on the WWW under http://dx.doi.org/10.1002/chem.200801428.

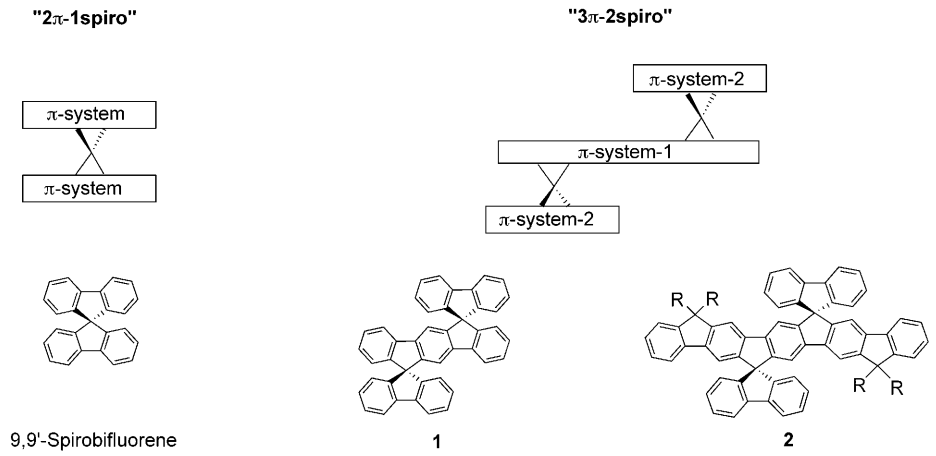

Figure 1. General molecular structure of spiro-linked molecules (from Salbeck and co-workers[8]): the 2π-1spiro concept (left). Molecular design adopted in this work: the 3π-2spiro concept (right).

(DSF-IF), for use in OLED applications.[28–30] The "3π-2spiro" architecture of these molecules (Figure 1) preserves the π conjugation of the indenofluorene core, that is, π-system-1, which plays a prominent role in their electronic and electrochemical properties. The introduction of the spiro-linked fluorene rings, that is, π-system-2 units, gives the molecules a highly rigid structure. Contrary to 2π-1spiro compounds,[8] 3π-2spiro compounds have only been reported on a few occasions.[27,31,32] For example, Bo and co-workers recently reported monodisperse ladder-type oligomers with two, three, four and seven spiro bridges using an elegant approach involving the oxidation of the fluorene C-9 carbon atom as a key step.[26]

On the other hand, aromatic diketones such as fluorenone derivatives and their corresponding more conjugated analogues are good electron-accepting materials and have recently received attention as electron-transport materials (ETMs) in OLEDs and as n-type materials for photovoltaic applications.[21,33–35] For example, new indenofluorenone- and bisindenofluorenone-based molecular building blocks have recently been synthesized and appear to be a promising family for n-channel semiconducting polymers.[36]

In this context, we have proposed new routes to 3π-2spiro molecules using extended diketone derivatives as key intermediates. We have thus investigated a short and efficient new route to **1** starting from indeno[1,2-*b*]fluorene-6,12-dione (**3**) (Scheme 1, route b). This approach was extended to the synthesis of the dispirofluorene ladder pentaphenylene **2** starting from the corresponding extended diketone **10** (Scheme 1, route d). Herein, we first report our synthetic investigations towards these new oligomers as potential emitters for OLED applications. The thermal, structural, electrochemical, theoretical and optical properties of these oligomers and their corresponding diketone intermediates are then discussed. Finally, we present the behavior of oligomer **2** as an emissive layer within an OLED.

Results and Discussion

Synthesis: 9,9′-Spirobifluorene can be considered to be the fusion of two fluorene units through a shared spiro carbon and is readily obtained in a two-step synthesis from 2-halogenobiphenyl and fluorenone through a metal–halogen exchange reaction.[10,37–40] As **1** can be considered to be the fusion of two 9,9′-spirobifluorene moieties through a shared phenyl ring, our previous retrosynthetic analysis of **1** was based on a double lithium–halogen exchange reaction (Scheme 1, route a) and involved 2,2″-diiodo-1,1′;4′,1″-terphenyl (2,2″-DITP) as the key starting material.[29] Despite the efficiency of this route, it was, however, evident that a similar synthetic approach might not be used to prepare **2** because the preparation of the key diiodinated intermediate appeared to be highly complicated (Scheme 1, route c). Moreover, we have recently shown that, when the fluorenone core is substituted in the 2- and 7-positions, route a leads to positional isomers of DSF-IFs[30] and is therefore inadequate for the synthesis of **2**. Stimulated by the work of Müllen and Scherf and their co-workers, we thus decided to investigate a new route to 3π-2spiro molecules such as **1** (Scheme 1, route b), which may also be used for the synthesis of the more extended oligomer **2** (Scheme 1, route d). These two approaches were both based on a key coupling reaction between a diketone derivative, that is, **3** or **10**, and 2-halogenobiphenyl. A similar approach has recently been developed by Vak et al. for the synthesis of a polyindenofluorene bridged by two spiro anthracene fragments.[27]

Starting from the commercially available 2,5-dibromo-1,4-dimethylbenzene, the diketone **3** was prepared on the multigram scale in a three-step synthesis as previously reported.[29,41] As shown in Scheme 2, the lithium–iodine exchange of 2-iodobiphenyl[42] **4** with *n*-butyllithium at a low temperature followed by quenching with the diketone **3** afforded the dialcohol **5**, which was not purified at this stage and was immediately used in an intramolecular cyclisation reaction under acidic conditions, that is, AcOH/HCl, and led to compound **1** in a yield of 26% (not optimiszed). This new route, performed in an overall yield of 18%,[43] is short, efficient and highly adaptable to the preparation of various DSF-IF derivatives substituted either on the π-system-1 (substitution of the diketone **3**) or on the π-system-2 (substitution of the iodobiphenyl **4**).

In the light of these results, we decided to follow the same strategy to prepare the ladder-type pentaphenylene **2** (Scheme 3). In this context, the diketone **10** was the key intermediate. Suzuki coupling of the fluorene-2-boronate

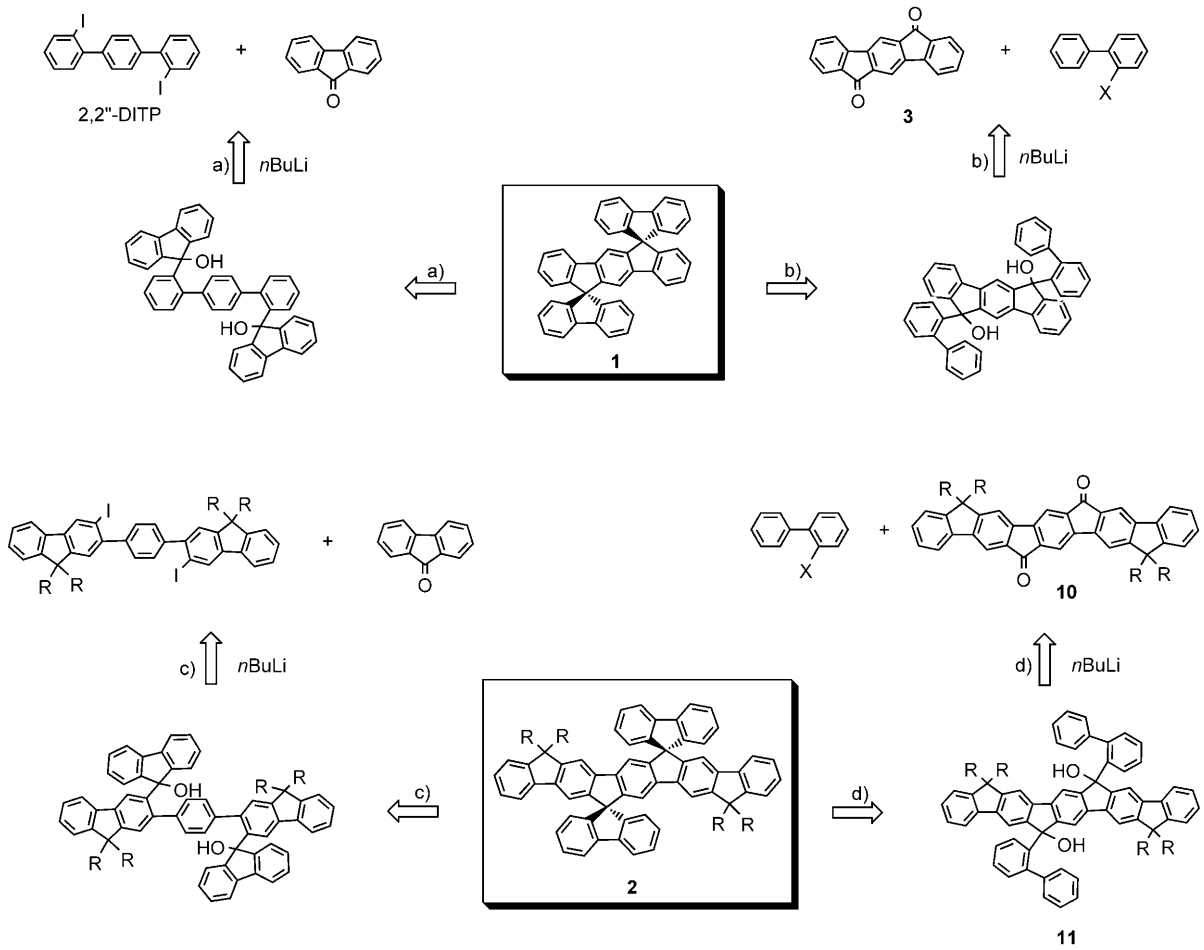

Scheme 1. Retrosynthetic approaches to dispiro **1** and **2** (X = Br, I; R = C_8H_{17}).

7[44–46] and the dibromoterephthalate **6**[47] generated the key intermediate **8** (see the Supporting Information for full details of the syntheses), previously reported with a methyl ester group by Müllen and co-workers.[21] In the solid state (see the molecular structure of **8** from single-crystal X-ray diffraction data in the Supporting Information), the two fluorene rings of **8** lie on each side of the central phenyl ring with angles of around 50.8°. The shortest distance between the carbon atom of the carbonyl group and the corresponding adjacent carbon atom in the fluorene ring is 3.1 Å. Unfortunately, acidic treatment of **8**, as previously described for similar structures, that is, in concentrated H_2SO_4 at 165 °C,[21,36] in AcOH/HBr at 110 °C[41] or in CH_3SO_3H at 65 °C,[48] failed to produce **10**. Saponification of the diester **8** under basic conditions (NaOH/EtOH at reflux) readily provided the corresponding terephthalic acid **9**, which was converted into the corresponding acid dichloride (oxalyl chloride, DMF, RT). Finally, Lewis acid promoted intramolecular Friedel–Crafts acylation ($TiCl_4$, 0 °C)[49] of the acid dichloride readily took place to give the diketone **10** in a yield of 91% over the two steps. With this key building block in hand, the last step required its coupling to the 2-metallobiphenyl. Note that this reaction appears to be difficult to perform and is highly sensitive to the reaction conditions, including magnesium versus lithium, iodobiphenyl versus bromobi-

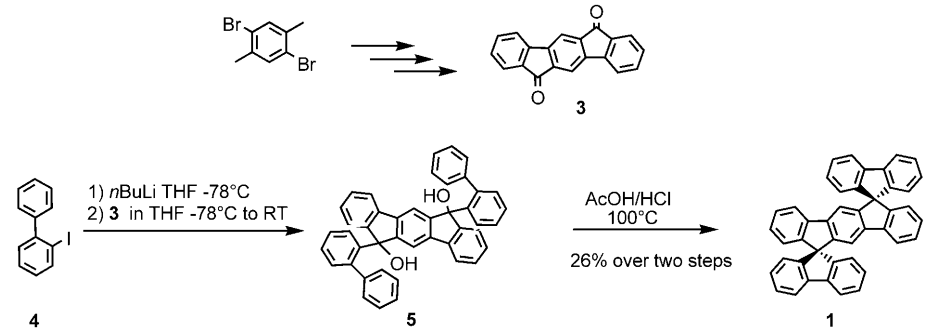

Scheme 2. Synthesis of DSF-IF **1**.

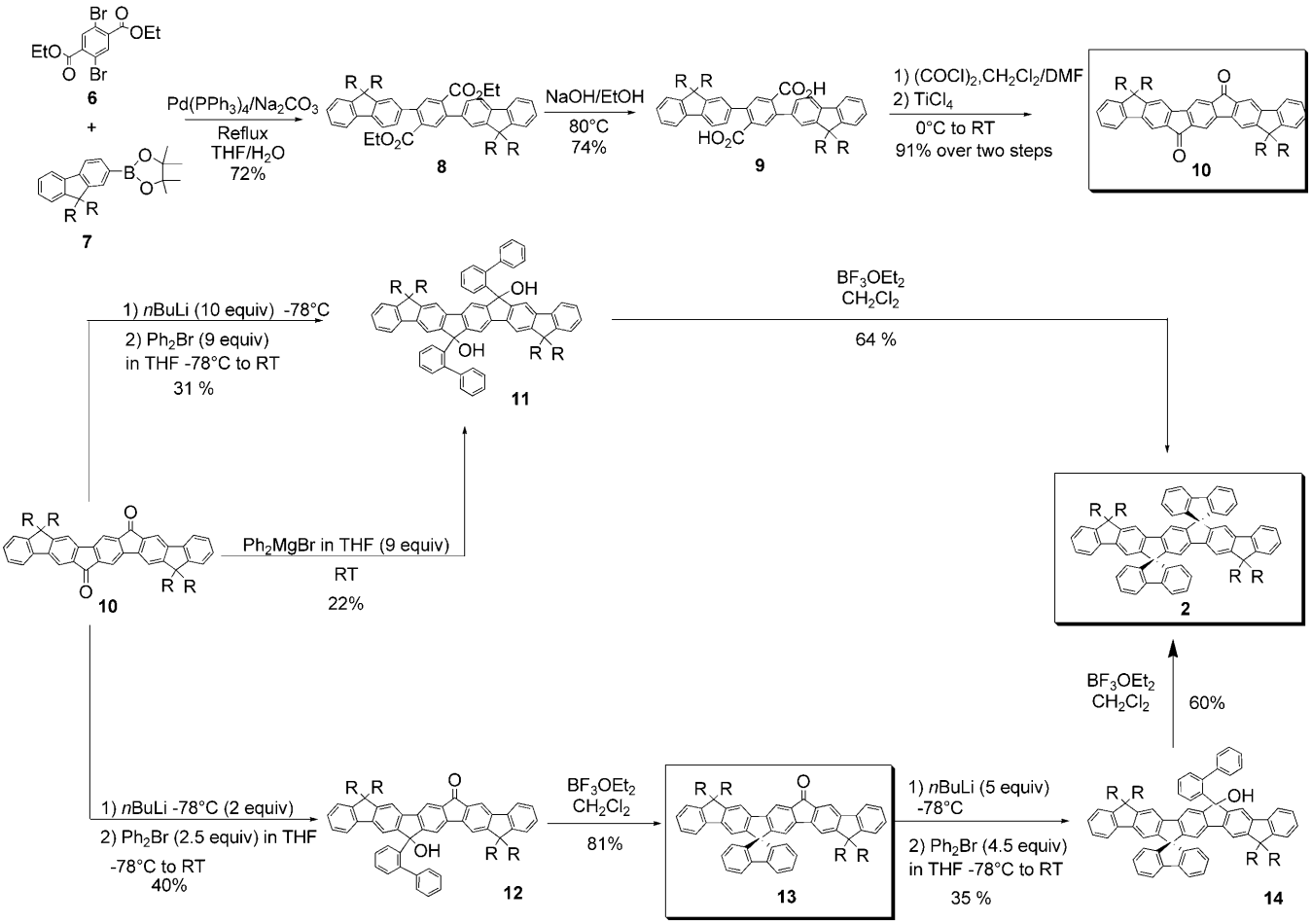

Scheme 3. Syntheses of **10**, **13** and **2** (R = C_8H_{17}, Ph_2Br = 2-bromobiphenyl).

phenyl, THF versus diethyl ether, the nature of the base and the time of formation.

After several attempts, the dialcohol **11** was finally obtained in a yield of 31 %[50] and cyclized under mild conditions, that is, BF_3•OEt_2 in dichloromethane, to provide the expected 3π-2spiro pentaphenylene **2**.[51]

This coupling reaction can also be stopped at the monoalcohol **12** (Scheme 1), which can then be cyclized to give the monospiro monoketone derivative **13**. An extra biphenyl linkage was introduced by using the same conditions (see above) and led to the final dispiro **2** via the corresponding alcohol **14** (not isolated). The structure of **2** was confirmed by HMBC spectroscopy. Indeed, we recently showed that spiro carbon atoms are powerful probes for detecting neighboring hydrogen atoms through long-range shift correlations.[30] As expected, three cross-peaks were detected for the spiro carbon atoms, which correspond to three bond correlations (^3J) with the three neighboring hydrogen atoms (in CD_2Cl_2: δ = 7.20 (s), 6.98 (s), 6.88 ppm (d); see the figure in the Supporting Information). Note that the hydrogen atoms of the biphenyl linkages in alcohols **11** and **12** appear as broad signals in the ^{1}H NMR spectra (see the Supporting Information). This feature was attributed to the slow rotation of the biphenyl moieties due to a sterically hindered environment. The monoketone **13** appeared to be an interesting model compound to study the electronic properties of 3π-2spiro derivatives. It is also a key intermediate for the synthesis of mixed 3π-2spiro molecules with two different π-system-2 moieties. Indeed, with an accurate molecular design, that is, electron-donating and/or -withdrawing substituents, these mixed structures may present highly interesting charge balance properties. Note that compounds **10**, **13** and **2** exhibit good solubility in common organic solvents, such as $CHCl_3$, CH_2Cl_2, THF and DMF.

Physicochemical properties of DSF-IF derivatives

Structural properties: Single crystals of **2** were obtained from a solution in $CDCl_3$ and analyzed by X-ray diffraction to elucidate its molecular structure and packing characteristics. The structure of **2** is presented in Figure 2. To the best of our knowledge, the characterisation of this kind of long ladder-type *p*-phenylene derivative by X-ray crystallography has only been reported once by Wong et al. in 2006.[53] Compound **2** presents a linear antarafacial geometry[32] and its π-system-1 (19.4 Å long) does not adopt a strict coplanar con-

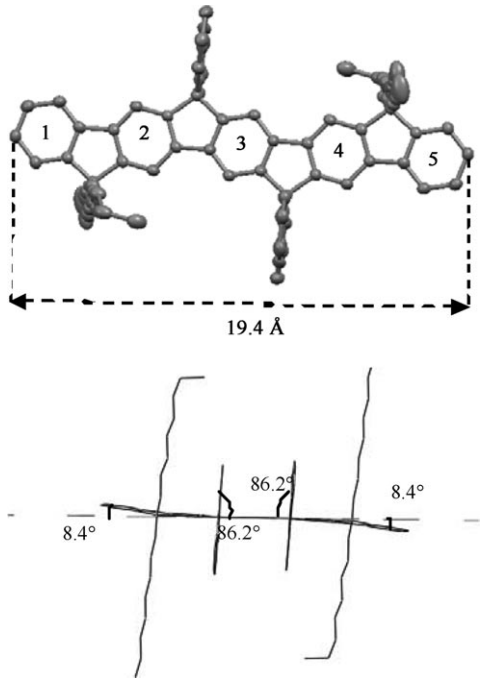

Figure 2. Views of the molecular structure of **2** from single-crystal X-ray diffraction data (hydrogen atoms have been omitted for clarity).

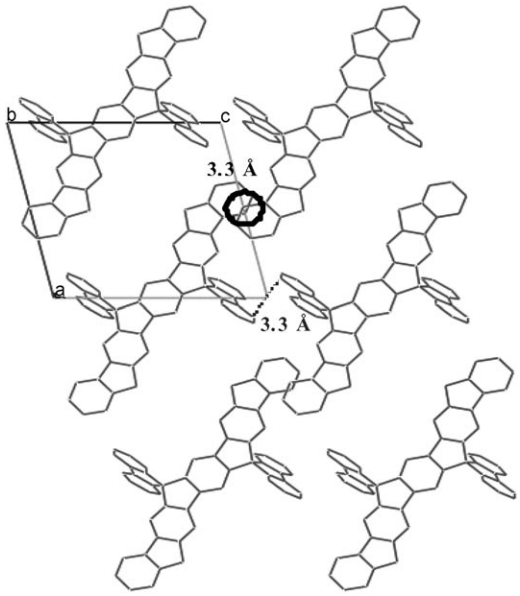

Figure 3. Crystal-packing diagram of **2** along the *b* stacking axis. The alkyl chains and the hydrogen atoms have been omitted for clarity.

figuration as two distortions exist on both sides. The dihedral angles between the plane of the central phenyl ring 3 and those of side rings 1 and 5 are 8.4° (see the labelling of the phenyl rings in Figure 2). These distortions are larger than those reported by Wong et al.,[53] that is, 2.5°, for an analogous tetra *p*-tolyl-substituted ladder-type oligo-pentaphenylene. The angle between the plane of the central phenyl ring 3 of π-system-1 and that of π-system-2 (through the central cyclopentane ring) is 86.2° (Figure 2).

As indicated in the crystal packing diagram of **2** shown in Figure 3, in which the alkyl chains have been omitted for clarity, the two π-system-2 moieties lie on either side of the π-system-1 plane. The closest C–C distance between two terminal phenyl rings of two neighboring molecules of the π-system-1 moieties was estimated to be 3.3 Å (Figure 3, plain circle). The closest C–C distance between two π-system-2 moieties of two neighboring molecules was also determined to be 3.3 Å (Figure 3, dashed line). Despite these two short distances, these packing diagrams indicate the lack of effective interchromophore π–π interactions in the solid state.

Electrochemical properties: The redox properties of the dispiro derivative **2** were investigated by cyclic voltammetry (CV). Diketones **3** and **10** and monoketone **13**, key intermediates in our synthetic approaches, were also electrochemically studied because they may be interesting as electron-accepting materials.[21,36,54] Electrochemical data are summarized in Table 1.

The oxidation of **2** recorded in CH_2Cl_2 between 0.3 and 2.25 V (Figure 4a) occurs in three steps, the maxima of which are at E^1_{ox} (1.09 V), E^2_{ox} (1.66 V) and E^3_{ox} (1.95 V). The

Table 1. Electrochemical data for **2**, **3**, **10** and **13** (vs. SCE).

	E^1_{ox} [V]	E^2_{ox} [V]	E^{onset}_{ox} [V]	E^1_{red} [V]	E^2_{red} [V]	E^{onset}_{red} [V]	HOMO [eV][a]	LUMO [eV][b]	ΔE^{El} [eV][c]
2	1.09	1.66	0.96	–	–	−2.3	−5.36	−2.1	3.26
3	1.70	–	1.65	−0.98	−1.38	−0.85	−6.05	−3.55	2.5
10	1.40	1.68	1.27	−1.07	−1.52	−0.92	−5.67	−3.48	2.19
13	1.23	1.56	1.06	−1.35	–	−1.15	−5.46	−3.25	2.21

[a] Calculated from the onset oxidation potential E^{onset}_{ox}. [b] Calculated from the onset reduction potential E^{onset}_{red}. [c] Calculated as $\Delta E^{El} = |HOMO - LUMO|$ from the redox data.

first oxidation E^1_{ox} is reversible (Figure 4c) and occurs in a potential range similar to that observed for analogous coplanar penta-*p*-phenylene oligomers reported by Wong,[53] Bo[26] and Müllen[25] and their co-workers. This process has been assigned to the formation of a radical cation delocalized throughout the π-system-1. The potential difference between the first oxidation potential E^1_{ox} of **1**[29] (1.47 V) and **2** (1.09 V) is around 0.38 V, which clearly shows the extension of conjugation of the π-system-1 in **2**. The second oxidation wave (Figure 4b) is multi-electronic and the intensity ratio of E^1_{ox}/E^2_{ox}, measured in the first scan, is around 1:4. This process was assigned to the second oxidation of the π-system-1, which leads to a dication, as has also been observed for other coplanar penta-*p*-phenylene derivatives,[25,26,53] concomitant with the oxidation of the two spiro-linked π-system-2 moieties. Indeed, this second wave E^2_{ox} (1.66 V) corresponds well with the primary oxidation waves of fluorene and 9,9′-spirobifluorene centered at 1.62 and 1.69 V, respectively.[29] This behavior led us to conclude that the radical cation is highly stable and strongly delocalized throughout the π-system-1 and that there is no or very little charge transfer between π-system-1 and the two π-system-2

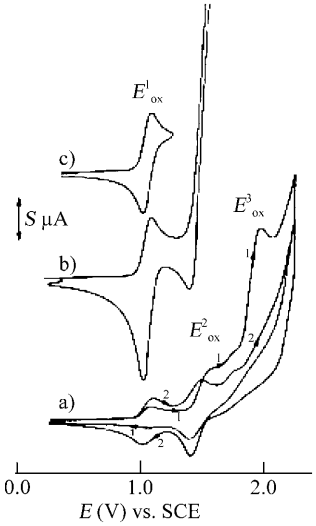

Figure 4. CV traces of **2** (2×10^{-3} M) in CH_2Cl_2 (0.2 M Bu_4NPF_6). Working electrode: platinum disk, diameter 1 mm; sweep rate: 100 mV s^{-1}. The scanning potential window was 0.3–2.25 V (two cycles) in (a), 0.3–1.52 V in (b) and 0.3–1.2 V in (c) (one cycle). The current scale S is equal to 4 μA in (a) and to 0.8 μA in (b) and (c).

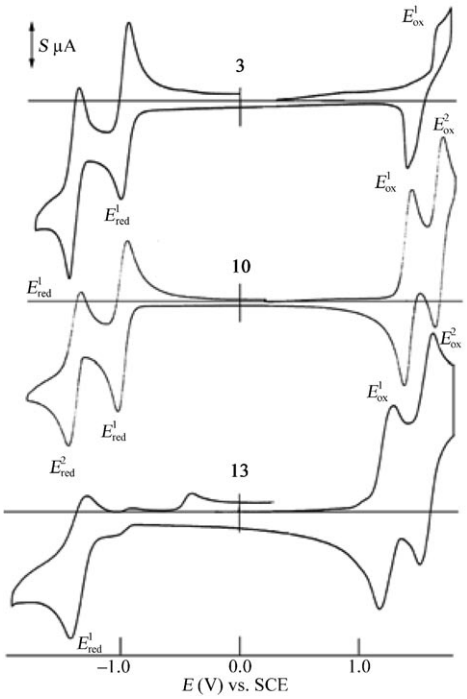

Figure 5. CV traces of **3** (1.13×10^{-2} M), **10** (1.1×10^{-3} M) and **13** (10^{-3} M) in CH_2Cl_2 (0.2 M Bu_4NPF_6). Working electrode: platinum disk, diameter 1 mm; sweep rate 100 mV s^{-1}. The scanning potential window was 0.0–1.8 V and back to −1.75 V for **3**, −1.8 V for **10** and −1.95 V for **13**. The current scale S is equal to 0.4 μA for **3** and 0.8 μA for **10** and **13**.

moieties. For **1**, the second oxidation maximum E^2_{ox} is shifted to 1.95 V due to charge transfer from the π-system-1 radical cation to the neutral π-system-2. Consequently the π-system-2 is more difficult to oxidise. Recurrent cycles in a potential range that includes the two E^1_{ox} and E^2_{ox} waves of **2** do not lead to any electrodeposition, contrary to what was observed for **1**. The absence of electropolymerisation of **2** might be explained by the high stability of the radical cation delocalized throughout the π-system-1 and by the sterically hindered environment of the π-system-2 moieties (see the crystal structure determined from the X-ray diffraction data in Figure 3). The reduction of **2**, close to the dichloromethane electrolyte discharge, was detected as a threshold at −2.3 V.

The diketone **3**[35] presents an ill-defined wave with a maximum E^1_{ox} centered at 1.70 V. The diketone **10** and the monoketone **13** show two reversible oxidation waves with maxima at 1.40/1.23 V (E^1_{ox}) and 1.68/1.56 V (E^2_{ox}), respectively (Figure 5). Compared with **2**, the presence of one (for **13**) and two (for **10**) electron-withdrawing carbonyl groups causes their first oxidation potentials to be shifted to more anodic values by around 0.17 and 0.31 V, respectively. The oxidation of **10** and **13** leads to the formation of radical cations and dications that are stable on the CV timescale, as shown by the successive reversible mono-electronic oxidation waves. Moreover, a comparison of E^1_{ox} for **3** (1.70 V) and **10** (1.40 V) shows the extended π delocalisation of the phenylene ladder backbone from three to five phenyl units (in **3** and **10**, respectively). Note that under the same experimental conditions, 9-fluorenone presents a first reversible oxidation wave with a maximum centered at 2 V (vs. SCE), see the Supporting Information for details. In the cathodic range, the diketones **10** and **3** present two reversible reduction waves leading to stable radical anions, which reveals interesting electron-accepting properties. The value of E^1_{red} for **10** (−1.07 V) is consistent with the first reduction potential of the analogous diketone, slightly more extended, described by Müllen and co-workers (−1 V).[21] Relative to the less extended diketone **3** ($E^1_{red}=-0.98$ V), the value of E^1_{red} for **10** is shifted to more negative values. This shift may be attributed to a less efficient electron-withdrawing effect of the two carbonyl groups on a more extended aromatic backbone. As expected, the presence of only one carbonyl group in compound **13** leads to a negative shift of the first reduction potential compared with that of **10**.

Theoretical calculations[55] are consistent with the electrochemical measurements, pointing to π-system-1-based primary oxidation and reduction in **2**, as shown by the nature of the frontier molecular orbitals (Figure 6).[56] Indeed, the HOMO and LUMO show π-system-1 character. This was also observed in the case of **1**.[29] The two pairs of quasi-degenerate LUMO+1 and LUMO+2 show π-system-2 character. The HOMO−1 has mixed character, whereas the HOMO−2 has mainly π-system-2 character. The electron affinity (LUMO energy) and ionisation potential (HOMO energy) have been estimated from the redox data (Table 1).[57,58] The estimated HOMO and LUMO energies for **2** are −5.36 and −2.1 eV, respectively, determined by using an SCE energy level of 4.4 V relative to vacuum. Relative to **1** (HOMO: −5.76 eV; LUMO: −2.17 eV, $\Delta E^{El}=$ 3.59 eV),[29] the LUMO of **2** has the same energy. However, the HOMO of **2** is more strongly affected due to the extend-

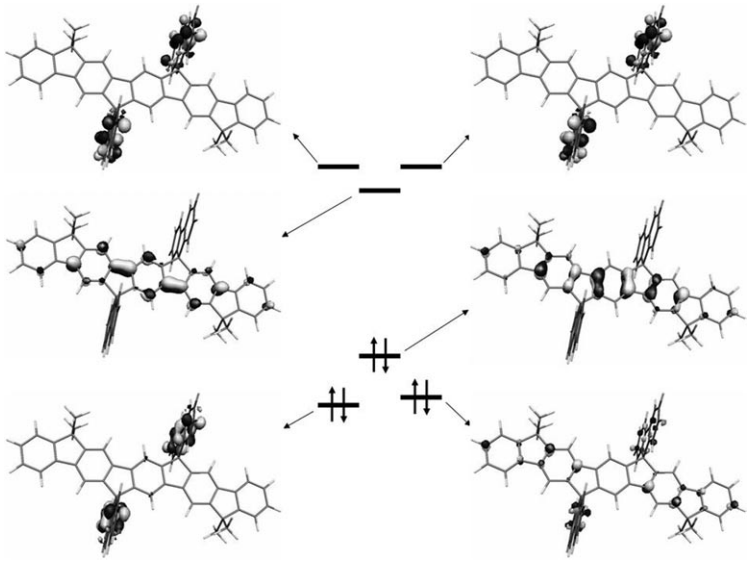

Figure 6. Sketch of frontier molecular orbitals for a simplified model of **2** (methyl instead of octyl groups) from Gaussian 03 B3LYP/6-31G* calculations.[56,59,60]

ed conjugation of the π-system-1 and lies 0.4 eV higher than the HOMO of **1**. Consequently, for OLED application, the energy level of the HOMO in **2** would be better suited to hole injection from the ITO/poly(3,4-ethylenedioxythiophene) (PEDOT) anode (see Figure 12). Thus, and compared with **1**, dispiro **2** possesses a smaller band gap, estimated at 3.26 eV.

Owing to the electron-withdrawing effects of their carbonyl groups, **3**, **10** and **13** each possess a low-lying LUMO. As observed by Müllen and co-workers,[21] we note that the LUMO energies of **10** and **3** fit well with metal cathodes such as magnesium (work function: −3.7 eV), which means that the injection of electrons should be favored in such devices. This latter point is of great interest as it may prevent the use of the highly reactive calcium cathode. To date there are still only a few ETMs that efficiently function as hole-blocking materials as well. For example, tris(8-hydroxyquinolinolato)aluminium(III) (Alq3, HOMO: −5.6 eV; LUMO: −3.1 eV), a well-known ETM, does not work efficiently as a hole blocker.[1] In this context, the diketone **3** appears to be interesting because its HOMO level is very low (−6.05 eV), which gives this molecule hole-blocking properties. However, the low solubility of **3** in common organic solvents is still an important issue that must be solved before practical application.[61]

Optical properties: The normalized solution UV/Vis absorption spectra of ladder-type oligomers **1** and **2** and their corresponding ketones **3**, **10** and **13** are presented in Figure 7 and the absorption data in Table 2. Diketone **3** possesses a strong absorption band with a maximum at 289 nm and a shoulder at a lower wavelength. It also possesses weaker absorption bands at 335 and 485 nm.[35] The main absorption band for **3** (289 nm) is blueshifted by 45 nm from the indenofluorene main absorption band (334 nm).[62] Three absorption bands have also been described previously in the literature for fluorenone[63] (assigned to π–π* transitions) and analogous diketones of **3** (assigned to π–π* and n–π* transitions).[21,36,61]

In the case of **10**, a similar strong absorption band is observed, redshifted to 326 nm, which clearly shows the extended conjugation. This strong absorption band also presents a shoulder at a lower wavelength.[21] The monoketone-monospiro **13** presents a similar band at 322 nm, but with a significantly lower intensity, because **13** possesses only one carbonyl group. Owing to the presence of two chromophores, that is, pentaphenylene and aryl ketone, **10** and **13** also present absorption bands typical of a pentaphenylene ladder-type oligomer[22,26] at 363/381 nm and

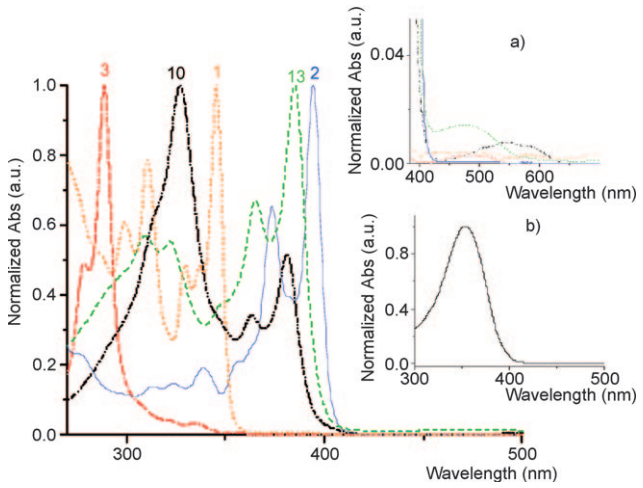

Figure 7. UV/Vis spectra of **1** (orange), **2** (blue), **3** (red), **10** (black) and **13** (green) in CH_2Cl_2 (10^{-5} M). Inset: a) The 400/650 nm portion; b) UV/Vis spectrum of ter-9,9′-dibutylfluorene in solution in CH_2Cl_2 (10^{-5} M).

Table 2. UV/Vis data and decomposition temperatures T_d for **1**–**3**, **10** and **13**.

	λ_{Abs} [nm][a]	T_d [°C][b]
2	230, 253, 263, 277, 312, 323, 339, 355, 373, 394	365
1[c]	231, 254, 300, 311, 330, 337, 345	355
3	227, 262, 279, 289, 335, 485	265
13	228, 309, 322, 365, 385, 474	345
10	228, 262, 326, 363, 381, 542	385

[a] Measured in CH_2Cl_2 (10^{-5} M). [b] Decomposition temperatures T_d corresponding to 5% loss, determined by thermogravimetric analysis (TGA). [c] From ref. [29].

365/385 nm, respectively. Very weak absorption bands were also observed at lower energy, around 474 nm for **13** and 542 nm for **10**, which correspond to symmetry forbidden n–π* transitions of the carbonyl function, as recently assigned by Müllen and co-workers (Figure 7, inset b).[33,54] At this stage, it should be stressed that the interpretation of the intrinsic optical properties of fluorenone incorporating polymer or oligomer still remains controversial.[64] The UV/Vis absorption spectrum of **2** presents a well-defined vibronic structure with two main absorptions at 373 and 394 nm, also observed in **1** (330 and 345 nm)[29] but bathochromically shifted by around 43/49 nm (optical band gap:[65] 3.07 eV for **2** vs. 3.51 eV for **1**). As this absorption arises from the central π-system-1, this clearly indicates that the degree of π conjugation has been effectively extended. The absorption maximum of **2** was also redshifted by around 40 nm relative to those of terfluorene derivatives (for example, ter(9,9′-dioctylfluorene)s: 352 nm;[66,67] ter(9,9′-dibutylfluorene)s: 354 nm (Figure 7, inset b);[68] ter(9,9′-diarylfluorene)s: 353–356 nm).[69] Moreover, and in contrast to the case of **2**, it is known that these terfluorene absorption bands are structureless due to the rotational freedom of the phenyl rings around the C–C bonds that link the fluorene units (Figure 7, inset b).[66] The same behavior was also observed with tetraoctylindenofluorene dimers and trimers with maximum absorptions in solution recorded at 371 and 383 nm, respectively.[70] These features clearly indicate the effectiveness of using fused architectures to increase the planarity and thus electronic delocalisation throughout the structure.

The photoluminescence of **2** was studied in cyclohexane (Figure 10). The emission maxima recorded at 397 and 420 nm are also redshifted compared with those of **1**, that is, 347 and 366 nm,[29] which indicates again the extension of the conjugation in π-system-1. These transitions have been assigned to 0–0 and 0–1 singlet transitions.[25] As expected, the Stokes shift is small and consistent with a highly rigid structure. The fluorescence quantum yield of **2** in solution[41] is very high (90% for **2** vs. 62% for **1**), which indicates that non-radiative decay pathways are nearly suppressed in such structures. Before discussing the behavior of **2** in OLEDs and to determine its stability against the formation of oxidative keto-type defects, spin-coated films of 3π-2spiro compounds **1** and **2** on quartz substrates were exposed to thermal stress conditions under an ambient atmosphere.

A comparison of the thin-film and solution fluorescence spectra of **1** reveals an 8 nm redshift between the two first emission peaks and a broader spectrum (Figure 8). This may be explained by the different dielectric constants of the two different environments.[18,71] Note that the intensity of the relative maxima in the solid state is highly dependent on the preparation conditions (vacuum deposition vs. spin-coated).[19,71] In our case the second and third bands (374/386 nm) in the solid state are higher in intensity than those in solution (355/365 nm). The UV/Vis thin-film spectrum of **1** (Figure 8) is almost identical to the solution spectrum[29] with only a slight bathochromic shift in the maximum from 344 to 349 nm.

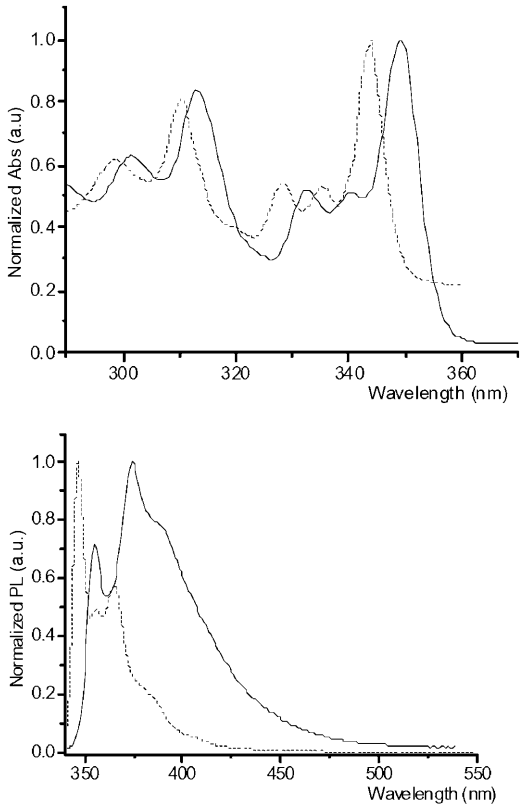

Figure 8. Absorption (top) and photoluminescence (bottom, λ_{exc} = 275 nm) of **1** in solution in cyclohexane (-----) and in thin film (——).

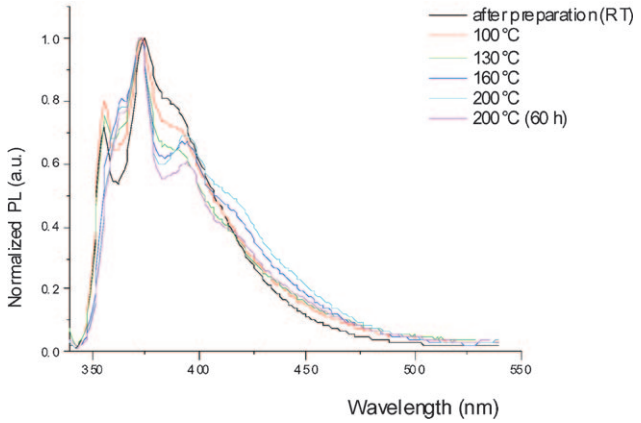

Figure 9. Normalized thin-film photoluminescent spectra of **1** after annealing for 1 h at different temperatures in air (λ_{exc} = 275 nm) and for 60 h at 200 °C.

The evolution of the fluorescence spectrum of **1** under thermal stress conditions is presented in Figure 9. Gradual heating of the spin-coated film in air from room temperature to 200 °C (1 h for each stage) did not lead to clear photoluminescent spectral changes. Even after 60 h at 200 °C, no signs of ketonic defect formations or aggregates (low-energy emission band beyond 500 nm) were detected.

The UV/Vis and thin-film fluorescence spectra of **2** present a fine vibronic structure and are almost identical to their

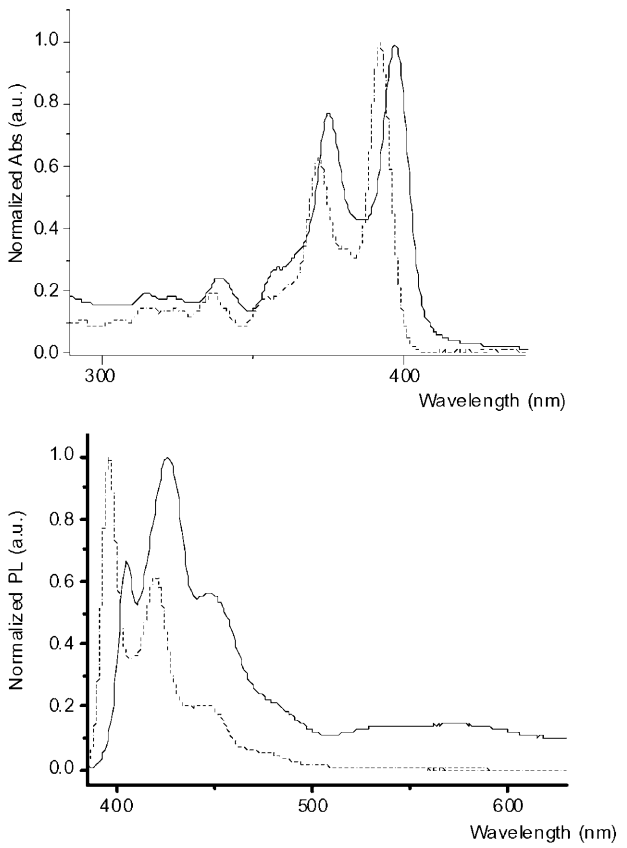

Figure 10. Absorption (top) and photoluminescence (bottom, $\lambda_{exc}=$ 320 nm) spectra of **2** in solution (cyclohexane, -----) and as a thin film (——).

solution spectra, being redshifted by only around 5 and 9 nm, respectively (Figure 10). However, and as observed for **1**, compared with the solution spectrum, the thin-film emission spectrum of **2** is broader and the intensity of the second fluorescence band appears to have a higher intensity. These results are consistent with those recently reported by Müllen and co-workers on a similar compound.[25] However, in the thin-film fluorescence spectrum a broad band appears between 500 and 600 nm. The intensity of this band increases slightly under thermal stress (RT to 200 °C, Figure 11) in an ambient atmosphere. Müllen and co-workers have demonstrated that fully alkylated poly(indenofluorene) and ladder-type poly(pentaphenylene) exhibit less stability towards oxidative degradation than their aryl counterparts as a result of the dialkyl bridgeheads, which are sensitive to oxidation.[2,22,24,72] Moreover, Bo and co-workers recently reported an identical thermal stress study of an analogous pentaphenylene derivative with four spiro-linked fluorenes at the bridges (no dialkyl bridgeheads). By heating a thin film up to 200 °C they reported no evident photoluminescent spectral change.[26] In addition, Bredas and co-workers have also investigated in depth the oxidative degradation process that occurs in ladder-type poly-*p*-phenylene bearing either a hydrogen atom or a methyl group (in addition to an aryl group) at the bridge.[73] Despite a significant decrease in the degree of degradation, ladder-type poly-*p*-phenylene with a

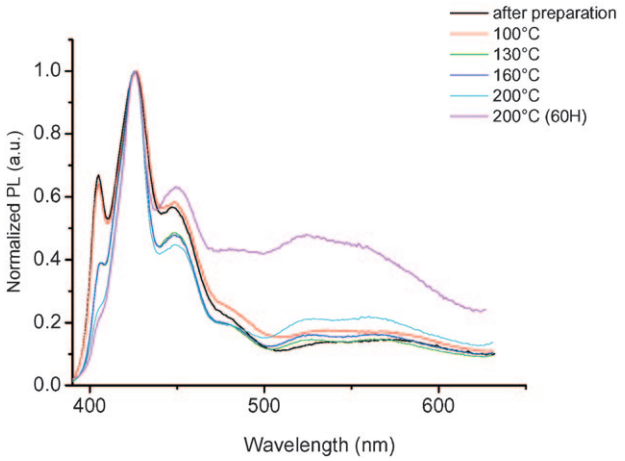

Figure 11. Normalized thin-film photoluminescent spectra of **2** after annealing for 1 h at different temperatures in air ($\lambda_{exc}=320$ nm) and for 60 h at 200 °C.

methyl group at the bridges is chemically degraded, which leads to the well-known low-energy emission. With all these recent findings, and as **1** did not present any low-energy emission, we assume that the dialkyl bridgeheads in **2** are responsible for the appearance of this long-wavelength emission band. It is then likely that the introduction of aryl groups instead of alkyl groups at the bridgeheads will resolve this issue.

Thermal properties: The thermal properties were evaluated by thermogravimetric analysis (TGA) under a nitrogen atmosphere at a rate of 5 °C min^{-1} (Table 2). The decomposition temperature (T_d, corresponding to 5% loss) increases significantly in the ketone series as the chain length increases (135 °C for 9-fluorenone, 265 °C for **3**, 385 °C for **10**; see the Supporting Information). Dispiro **2** also exhibits good thermal stability with a high T_d (365 °C), which is highly important for improving the lifetime of OLEDs.

OLEDs using 2 as the emitting layer: Various OLED structures were fabricated by using **2** as the emitting layer. At first, basic structures using ITO as the anode, PEDOT doped with poly(styrene sulfonate) (PSS) as the hole injecting layer (HIL), **2** as the emitting layer (EML) and calcium as the cathode were elaborated. As the LUMO of **2** is very low (−2.1 eV), a cathode with a low work function such as calcium (−2.9 eV) was used to enable charge injection into the emitting layer **2** (Figure 12a).

A comparison of the basic devices made from both spin-coated and evaporated films of **2** was carried out. Different solvents were used for the spin-coating: xylene, chloroform, 1,2-dichlorobenzene and cyclohexanone. Cyclohexanone appeared to be the best solvent for **2** when heated above 45 °C and allowed uniform films to be made, whereas the use of other solvents resulted in poor quality films. Thus, the devices made by spin-coating used cyclohexanone as the solvent. OLEDs were made by using different layer thicknesses for

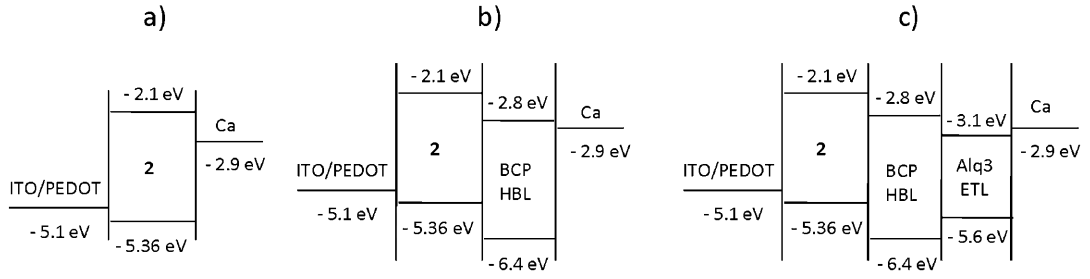

Figure 12. Schematic representation of the energy band diagram associated with the OLED devices investigated (before contact). HBL and ETL refer to the hole-blocking layer and the electron-transporting layer, respectively.

the emitting layer. Luminance–voltage characteristics for 60 and 120 nm thick emitting layers deposited by evaporation and spin-coating are displayed in Figure 13. Irrespective of

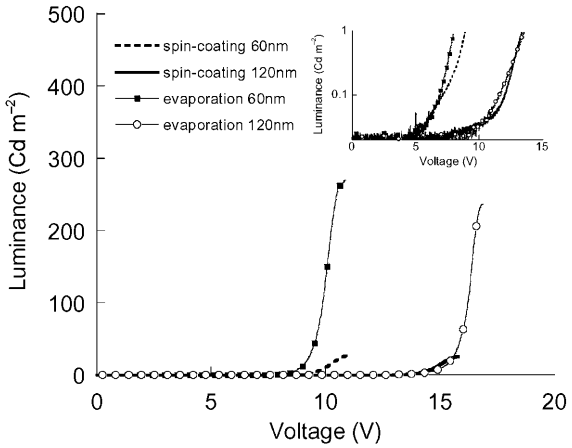

Figure 13. Luminance–voltage characteristics of ITO/PEDOT/**2**/Ca devices in which **2** was deposited by spin-coating and evaporation.

the deposition process, the turn-on voltage remained unchanged for an equivalent thickness (see the semi-logarithmic graph displayed in the insert of Figure 13). However, spin-coated and evaporated films exhibited very different behavior. Film prepared by the evaporation process led to luminance ten times higher than that observed for films formed by the spin-coating process. This is due to the quality of the film (see images of the surface in the Supporting Information). Indeed, the evaporation process leads to an almost defect-free film. In contrast, the need to use a warm solvent to perform the spin-coating makes it difficult to prevent the formation of aggregates when the solution is deposited onto the cold substrate. This results in poorer quality films and as a consequence in poorer performances.

To improve the performances of the devices, a hole-blocking layer (HBL) of 2,9-dimethyl-4,7-diphenyl-1,10-phenanthroline (bathocuproin, BCP), was evaporated between the emissive layer and the calcium cathode (Figure 12b). The low HOMO level of BCP (−6.4 eV) was intended to prevent holes from crossing the device and reaching the calcium cathode without recombination. Furthermore, to improve the transport of electrons, an electron-transport layer (ETL) of tris(8-hydroxyquinolinolato)aluminium(III) (Alq3) was thermally evaporated on top of the BCP, which resulted in devices with the following structure ITO/PEDOT/**2**/BCP/Alq3/Ca (Figure 12c).

The luminous efficiencies of the ITO/PEDOT/**2**/Ca, ITO/PEDOT/**2**/BCP/Ca and ITO/PEDOT/**2**/BCP/Alq3/Ca devices are compared in Figure 14. The BCP-based OLED ex-

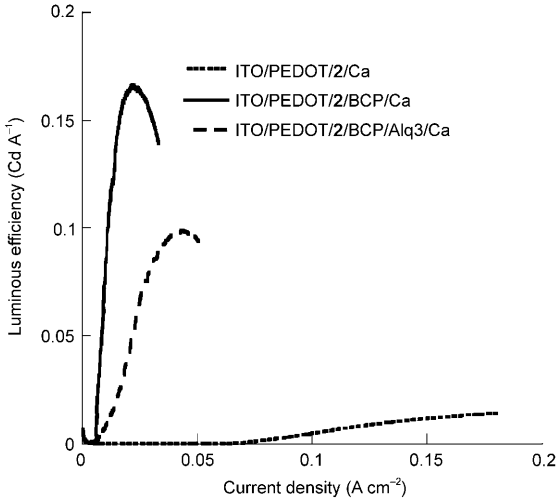

Figure 14. Luminous efficiency versus current density for the ITO/PEDOT/**2**/Ca, ITO/PEDOT/**2**/BCP/Ca and ITO/PEDOT/**2**/BCP/Alq3/Ca OLEDs.

hibits the best performance. The energy-band diagram in Figure 12b shows that the energy barrier between the HOMO levels of **2** and BCP is 1 eV, which is sufficient to block of holes and confine them to the emitting layer. This results in an increase in radiative recombination and therefore an enhancement in the performance of the BCP-based OLED compared with the single layer device. Indeed, without BCP, holes can cross the emitting layer to the calcium electrode without radiative recombination, which would reduce the efficiency.

The insertion of Alq3 above BCP slightly reduces the luminous efficiency from 0.16 to 0.1 Cd A^{-1}. This shows that **2** enables the transport of electrons without the need for an additional ETL. Alq3 does not favor the transport of electrons in the emissive layer from the calcium cathode as the LUMO level of BCP (−2.8 eV) perfectly fits the work func-

tion of calcium (−2.9 eV). Thus the optimum OLED structure is ITO/PEDOT/**2**/BCP/Ca. The associated current density–luminance–voltage curves are displayed in Figure 15 with a turn-on voltage of 8 V (measured precisely by using the semi-logarithmic plot) and a maximum luminance of 470 Cd m^{-2}.

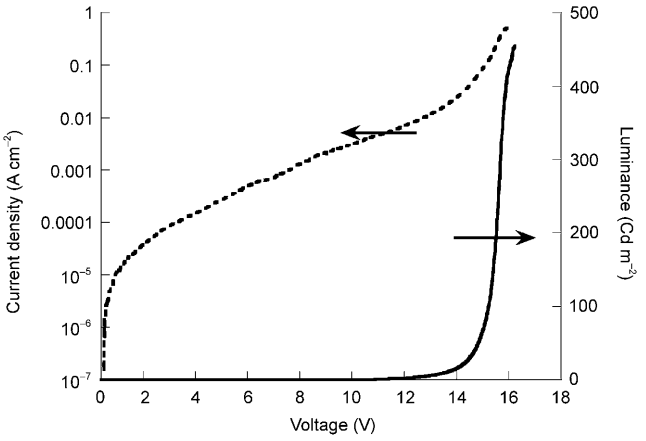

Figure 15. Current density–luminance–voltage characteristics of an ITO/PEDOT/**2** (100 nm)/BCP/Ca OLED.

The normalized electroluminescence spectrum recorded for the ITO/PEDOT/**2**/BCP/Ca device (Figure 16a) reveals three main emission peaks, two very sharp peaks at 404 and 427 nm and one much broader centered around 560 nm. A fourth minor contribution can be observed at 452 nm. At low wavelengths the emission spectrum of the OLED is very similar to the thin-film fluorescence spectrum of **2**. The contribution at 560 nm seems to correspond to the broad fluorescence band that appeared between 500 and 600 nm when the sample was heated at 200 °C for 60 h. However, it seems difficult to correlate these two bands (ambient atmosphere vs. inert atmosphere) and further studies on the exact nature of this emission are required. The chromatic coordinates calculated from the electroluminescence spectrum in the CIE 1964 chromaticity diagram are (0.30, 0.27), as can be seen in Figure 16b.

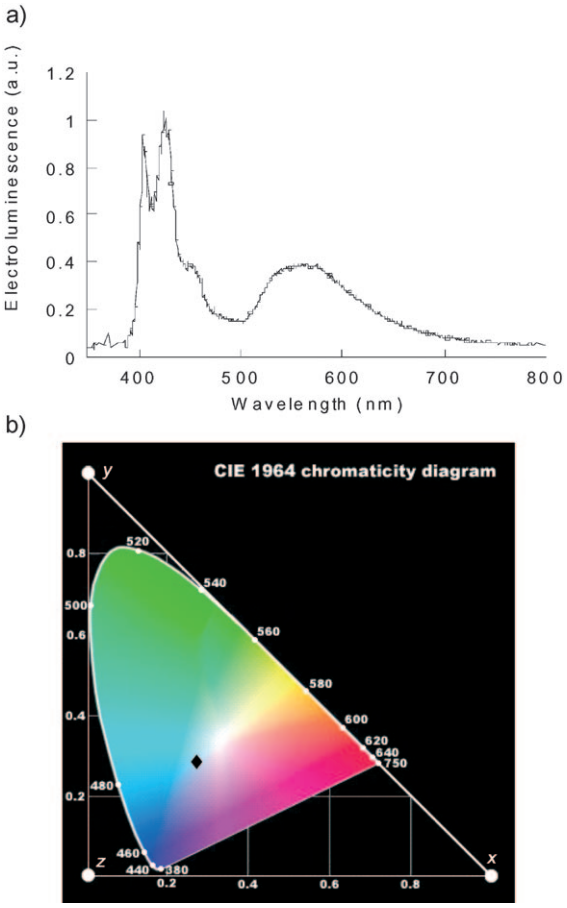

Figure 16. a) Normalized electroluminescence spectrum of the ITO/PEDOT/**2**/BCP/Ca OLED; b) corresponding color on a CIE 1964 chromaticity diagram.

Conclusions

We have developed new efficient routes to the synthesis of 3π-2spiro ladder-type oligomers **1** and **2** by using extended diketone derivatives as key intermediates. The structural, electrochemical, thermal and optical properties of **2** have been studied in detail and compared with the less extended oligomer **1**. Because the π-system-1 conjugation increases on going from **1** to **2**, we logically observed a band-gap contraction from 3.59 eV for **1** to 3.26 eV for **2**. Compound **2** exhibited intense fluorescence and a very small Stokes shift in solution as well as in the spin-coated thin film due to the rigidity of the backbone. The OLED application studies were carried out with **2** as the emissive layer. Although the devices displayed moderate efficiencies, the use of a hole-transporting layer could be avoided because the HOMO level of **2** fits well with the work function of the anode ITO/PEDOT. The electroluminescence spectrum of **2** showed two blue contributions (404 and 427 nm) and an additional low-energy emission band (560 nm), which leads to chromatic coordinates of (0.30, 0.27). After the application of thermal stress in the presence of oxygen, a low-energy emission band was also observed in solid-state fluorescence studies. However, the relationship between these low-energy bands, obtained under either an ambient or inert atmosphere, is not evident as they may arise from different causes. Further studies are currently underway in our laboratory to determine the exact nature of these low-energy emissions.

Experimental Section

Synthesis: Commercially available reagents and solvents were used without further purification except for those detailed below. Dichloromethane and acetonitrile were distilled from the P_2O_5 drying agent Sicapent (Merck). THF and diethyl ether, were distilled from sodium/benzophenone prior to use. Light petroleum refers to the fraction with b.p. 40–60 °C. Reactions were stirred magnetically, unless otherwise indicated. Analytical thin-layer chromatography was carried out by using alumini-

um-backed plates coated with Merck Kieselgel 60 GF_{254} and visualisation under UV light (at 254 and/or 365 nm). Chromatography was carried out by using silica 60A CC 40–63 μm (SDS). ^1H and ^{13}C NMR spectra were recorded by using Bruker 300 MHz instruments (^1H NMR frequency; the corresponding ^{13}C NMR frequency is 75 MHz). The chemical shifts are given in ppm and the *J* values in Hz. In the ^{13}C NMR spectra, the signals corresponding to CH, CH_2 and Me groups, assigned from DEPT experiments, are noted; all others are C. The residual signals for the NMR solvents are as follows: $CDCl_3$: $\delta = 7.26$ ppm for the proton and $\delta =$ 77.00 ppm for the carbon; CD_2Cl_2: $\delta = 5.32$ ppm for the proton and $\delta =$ 53.80 ppm for the carbon; $(CD_3)_2SO$: $\delta = 2.50$ ppm for the proton and $\delta =$ 39.43 ppm for the carbon. The following abbreviations have been used for the NMR assignments: s for singlet, d for doublet, t for triplet, q for quartet and m for multiplet; br refers to a broad signal. High-resolution mass spectra were recorded either at the Centre Régional de Mesure Physique de l'Ouest (Rennes) or with a Bruker Microflex LT spectrometer. 2-Iodobiphenyl was prepared according to a literature procedure.[42] Diketone **3** was prepared in a three-step synthesis as previously reported.[29,41] Full characterisation of DSF-IF **1** may be found in our previous work.[28] 9,9-Dioctylfluorene-2-boronate ester **7** was prepared according to literature procedures starting from the commercially available 2-bromofluorene.[44–46] Diester **6** was prepared by a modification of the Lamba and Tour procedure starting from 1,4-dibromo-2,5-dimethylbenzene in a two-step oxidation reaction followed by esterification (see the Supporting Information).[47] The names of chemicals have been generated with the naming service of ACD-I lab, which determines the chemical name according to systematic application of the nomenclature rules agreed upon by the International Union of Pure and Applied Chemistry and International Union of Biochemistry and Molecular Biology.

Dispiro[fluorene-9,6′-indeno[1,2-*b*]fluorene-12′,9″-fluorene] (1): 2-Iodobiphenyl (0.65 g, 2.34 mmol) was dissolved in dry THF (40 mL) in a Schlenk tube under an argon atmosphere. The solution was degassed and cooled to −78 °C before the dropwise addition, over 35 min, of *n*BuLi (1.6 M in hexane, 1.6 mL, 2.56 mmol). The resulting yellow solution was stirred for a further 55 min and diketone **3** (0.30 g, 1.06 mmol) partially dissolved in dry and degassed THF (100 mL) was added dropwise through a cannula. The reaction was stirred for 2 d (from −78 °C to room temperature) and the resulting mixture was poured into a saturated solution of ammonium chloride (15 mL) and extracted with CH_2Cl_2 (3× 50 mL). The extracts were dried ($MgSO_4$), the solvent was removed in vacuo and the residue was used in the next step without any further purification. Hydrochloric acid (5 drops) was added to a suspension of the crude mixture of difluorenol **5** in acetic acid (50 mL) and the resulting mixture was stirred for 2 h at 100 °C. After cooling to room temperature, water was added (20 mL) and a colorless solid was filtered and purified by column chromatography on silica gel eluting with CH_2Cl_2/light petroleum (2:8) to give **1** as a colorless solid (0.15 g, 26 %). The spectroscopic analyses and purity of **1** was in accordance with our previous work.[28]

Diethyl 2,5-bis(9,9-dioctyl-9*H*-fluoren-2-yl)terephthalate (8): Fluorene-2-boronate **7** (2.88 g, 5.56 mmol), potassium carbonate (0.84 g, 6.07 mmol), tetrakis(triphenylphosphine)palladium(0) (0.91 g, 0.1 mmol) and water (15 mL) were added to a solution of **6** (1.0 g, 2.6 mmol) in THF (30 mL) in a Schlenk tube. The Schlenk tube was degassed and the mixture was stirred at reflux under an argon atmosphere for 12 h. The cooled mixture was then extracted with diethyl ether (5×50 mL) and the extracts were washed with brine and dried ($MgSO_4$). The solvent was removed in vacuo and the residue was purified by column chromatography on silica gel eluting with CH_2Cl_2/light petroleum (1:9) to give **8** as a colorless solid (1.90 g, 72 %). ^1H NMR (300 MHz, $CDCl_3$): $\delta = 7.87$ (s, 2H; ArH), 7.77–7.74 (m, 4H; ArH), 7.39–7.32 (m, 10H; ArH), 4.10 (q, $J = 7.2$ Hz, 4H; OCH_2CH_3), 1.99 (t, $J = 7.2$ Hz, 8H; CH_2), 1.24–1.08 (m, 40H; CH_2), 1.00 (t, $J = 7.2$ Hz, 6H; OCH_2CH_3), 0.82 (t, $J = 7.2$ Hz, 12H; Me), 0.70–0.61 ppm (m, 8H; CH_2); ^{13}C NMR (75 MHz, $CDCl_3$): $\delta = 168.6$ (C), 150.93 (C), 150.89 (C), 141.2 (C), 140.7 (C), 140.6 (C), 138.9 (C), 133.9 (C), 131.5 (CH), 127.21 (CH), 127.17 (CH), 126.8 (C), 122.9 (CH), 122.8 (CH), 119.8 (CH), 119.4 (CH), 61.2 (CH_2), 55.2 (C), 40.4 (CH_2), 31.8 (CH_2), 30.1 (CH_2), 29.3 (CH_2), 23.8 (CH_2), 22.6 (CH_2), 14.0 (Me), 13.8 ppm (Me); IR (KBr): $\tilde{\nu} = 3056$, 2960, 2925, 2850, 1723 (C=O), 1466, 1383, 1227, 1131, 1109, 1020 cm^{-1}; HRMS (ESI): *m*/*z*: calcd for $C_{70}H_{94}O_4$+Na: 1021.70498 $[M+Na]^+$; found: 1021.7033.

2,5-Bis(9,9-dioctyl-9*H*-fluoren-2-yl)terephthalic acid (9): A solution of sodium hydroxide (10 N, 2.1 mL, 21.0 mmol) was added to a suspension of **8** (500 mg, 0.5 mmol) in ethanol (20 mL). The mixture was heated at reflux for 12 h. A solution of concentrated hydrochloric acid (37 %) was then carefully added dropwise until pH 1. Filtration gave **9** as a yellow solid (350 mg, 74 %). M.p. 203 °C (ethanol); ^1H NMR (300 MHz, [D$_6$]DMSO): $\delta = 13.06$ (br s, 2H; exch D_2O, OH), 7.88–7.81 (m, 4H; ArH), 7.75 (s, 2H; ArH), 7.45–7.30 (m, 10H; ArH), 1.99 (t, $J = 7.2$ Hz, 8H; CH_2), 1.17–1.01 (m, 40H; CH_2), 0.76 (t, $J = 7.2$ Hz, 12H; Me), 0.63–0.52 ppm (m, 8H; CH_2); ^{13}C NMR (75 MHz, [D$_6$]DMSO): $\delta = 168.8$ (C), 150.4 (C), 150.1 (C), 140.1 (C), 139.9 (C), 139.7 (C), 138.4 (C), 134.3 (C), 130.8 (CH), 127.2 (CH), 127.0 (CH), 126.8 (CH), 122.9 (CH), 122.7 (C), 119.8 (CH), 119.6 (CH), 54.6 (C), 31.0 (CH_2), 29.1 (CH_2), 28.4 (CH_2), 28.4 (CH_2), 23.2 (CH_2), 21.9 (CH_2), 13.8 ppm (Me), one CH_2 signal not observed; IR (KBr): $\tilde{\nu} = 3070$, 2963, 2927, 2850, 2650–2540, 1694 (C=O), 1460, 1430, 1407, 1287, 1243, 1128 cm^{-1}; HRMS (ESI): *m*/*z*: calcd for $C_{66}H_{86}O_4$+Na: 965.64238; $[M+Na]^+$; found: 965.6418.

9,9,18,18-Tetraoctyl-9,18-dihydrobenzo[5,6]-*s*-indaceno[1,2-*b*]indeno[2,1-*h*]fluorene-6,15-dione (10): Oxalyl chloride (201 mg, 134 μL, 1.59 mmol) and DMF (116 mg, 123 μL, 1.59 mmol) were added dropwise to a suspension of **9** (100 mg, 0.11 mmol) in CH_2Cl_2 (7 mL) and the solution was stirred at room temperature for 3 h. After removing the solvent in vacuo, CH_2Cl_2 (5 mL) was added and the solution was cooled to 0 °C before the addition of $TiCl_4$ (80 mg, 46 μL, 0.42 mmol). The dark mixture was stirred for 4 h at room temperature. The reaction was quenched with iced water (50 mL). The mixture was extracted with CH_2Cl_2 (3×20 mL) and the extracts were dried ($MgSO_4$). The solvent was removed in vacuo and the residue was purified by column chromatography on silica gel eluting with CH_2Cl_2/light petroleum (2:3) to give **10** as a grey solid (88 mg, 91 %). M.p. 226 °C (acetonitrile); ^1H NMR (300 MHz, $CDCl_3$): $\delta = 8.00$ (s, 2H; ArH), 7.86 (s, 2H; ArH), 7.72 (m, 2H; ArH), 7.52 (s, 2H; ArH), 7.39–7.36 (m, 6H; ArH), 2.03 (t, $J = 7.2$ Hz, 8H; CH_2), 1.26–1.07 (m, 40H; CH_2), 0.80 (t, $J = 7.2$ Hz, 12H; Me), 0.68–0.66 ppm (m, 8H; CH_2); ^{13}C NMR (75 MHz, $CDCl_3$): $\delta = 192.7$ (C), 159.5 (C), 150.6 (C), 146.0 (C), 143.1 (C), 142.8 (C), 140.0 (C), 139.7 (C), 133.7 (C), 127.9 (CH), 127.2 (CH), 122.9 (CH), 120.0 (CH), 115.9 (CH), 115.6 (CH), 115.2 (CH), 55.8 (C), 40.2 (CH_2), 31.7 (CH_2), 30.0 (CH_2), 29.2 (2×CH_2; determined by HMQC), 23.8 (CH_2), 22.6 (CH_2), 14.0 ppm (Me); IR (KBr): $\tilde{\nu} = 3052$, 2954, 2924, 2851, 1704 (C=O), 1605, 1421, 1273, 1143 cm^{-1}; UV/Vis (CH_2Cl_2): $\lambda_{max} = 381$ ($\varepsilon = 65589$), 363 (44657), 326 nm ($92069\ M^{-1}cm^{-1}$); HRMS (ESI): *m*/*z*: calcd for $C_{66}H_{82}O_2$: 906.63148; $[M]^+$; found: 906.6323; elemental analysis calcd (%) for $C_{66}H_{82}O_2$: C 87.36, H 9.11; found: C 87.42, H 9.32.

15-Biphenyl-2-yl-15-hydroxy-9,9,18,18-tetraoctyl-15,18-dihydrobenzo-[5,6]-*s*-indaceno[1,2-*b*]indeno[2,1-*h*]fluoren-6(9*H*)-one (12): 2-Bromobiphenyl (77 mg, 57 μL, 330 μmol) was dissolved in dry THF (20 mL) in a Schlenk tube under an argon atmosphere and the solution was degassed. The solution was cooled to −78 °C. *n*BuLi (1.6 M in hexane, 315 μL, 495 μmol) was added dropwise over 45 min. The resulting yellow solution was stirred for a further 45 min and diketone **10** (100 mg, 110 μmol), dissolved in dry, degassed and cooled (−78 °C) THF, was added dropwise through a cannula. The reaction was stirred overnight (from −78 °C to room temperature) and the resulting mixture was poured into a saturated solution of ammonium chloride (15 mL) and extracted with CH_2Cl_2 (3× 20 mL). The extracts were dried ($MgSO_4$), the solvent was removed in vacuo and the residue was purified by column chromatography on silica gel eluting with CH_2Cl_2/light petroleum (1:2) to give **12** as a red solid (47 mg, 40 %). ^1H NMR (300 MHz, $CDCl_3$): $\delta = 8.65$ (d, $J = 7.5$ Hz, 1H; ArH), 7.97 (s, 1H; ArH), 7.71–7.61 (m, 3H; ArH), 7.53–7.29 (m, 11H; ArH), 7.21 (s, 1H; ArH), 7.01 (d, $J = 7.5$ Hz, 1H; ArH), 6.87 (t, $J = 7.5$ Hz, 1H; ArH), 6.71 (br m, 1H; ArH), 6.53 (br m, 1H; ArH), 6.34 (br m, 1H; ArH), 6.08 (br m, 1H; ArH), 2.48 (s, 1H; exch D_2O, OH), 1.99 (m, 8H; CH_2), 1.34–1.08 (m, 40H; CH_2), 0.80 (t, $J = 7.2$ Hz, 12H; Me), 0.71–0.53 ppm (m, 8H; CH_2); ^{13}C NMR (300 MHz, $CDCl_3$): $\delta =$ 193.3 (C), 158.9 (C), 157.9 (C), 152.6 (C), 151.2 (C), 150.5 (C), 149.5 (C), 144.9 (C), 143.8 (C), 142.2 (C), 141.8 (C), 141.4 (C), 141.2 (C), 140.4 (C),

140.2 (C), 140.0 (C), 139.2 (C), 138.4 (C), 135.7 (C), 134.2 (C), 131.5 (CH), 129.3 (CH), 129.1 (CH), 127.6 (CH), 127.4 (CH), 127.3 (CH), 127.2 (CH), 127.1 (CH), 126.8 (CH), 126.5 (CH), 126.4 (CH), 125.8 (CH), 122.9 (CH), 122.8 (CH), 119.9 (CH), 119.8 (CH), 116.3 (CH), 115.7 (CH), 115.6 (CH), 114.9 (CH), 114.8 (CH), 81.9 (COH), 55.7 (C), 54.8 (C), 40.5 (CH_2), 40.3 (CH_2), 40.2 (CH_2), 40.0 (CH_2), 31.8 (CH_2), 31.7 (CH_2), 30.3 (CH_2), 30.0 (CH_2), 29.4 (CH_2), 29.2 (CH_2), 24.1 (CH_2), 23.8 (CH_2), 22.6 (CH_2), 22.5 (CH_2), 14.1 (Me), 14.0 ppm (Me); IR (KBr): $\tilde{\nu}$= 3056, 2925, 2853, 1715 (C=O), 1597, 1470, 1420, 1281, 1155 cm^{-1}; HRMS (ESI): *m/z*: calcd for $C_{78}H_{92}O_2$+Na: 1083.69950 $[M+Na]^+$; found: 1083.7001.

9,9,18,18-Tetraoctyl-9,18-dihydro-15*H*-spiro[benzo[5,6]-*s*-indaceno[1,2-*b*]-indeno[2,1-*h*]fluorene-6,9′-fluoren]-15-one (13): Compound **12** (160 mg, 0.15 mmol) was dissolved in CH_2Cl_2 (25 mL) and a solution of boron trifluoride diethyl etherate was added (76 μL, 86 mg, 0.60 mmol). The solution was stirred at room temperature for 10 min and the solvent was evaporated in vacuo. The residue was purified by column chromatography on silica gel eluting with CH_2Cl_2/light petroleum (1:2) to give **13** as a red solid (127 mg, 81%). ^{1}H NMR (300 MHz, $CDCl_3$): δ=8.19 (s, 1H; ArH), 7.99 (d, J=7.5 Hz, 2H; ArH), 7.94 (s, 1H; ArH), 7.82 (s, 1H; ArH), 7.68 (d, J=7.5 Hz, 1H; ArH), 7.49 (t, J=7.5 Hz, 2H; ArH), 7.41–7.17 (m, 10H; ArH), 7.02 (s, 1H; ArH), 6.91 (d, J=7.5 Hz, 2H; ArH), 6.86 (s, 1H; ArH), 2.05 (t, J=7.2 Hz, 4H; CH_2), 1.90 (t, J=7.2 Hz, 4H; CH_2), 1.27–0.99 (m, 40H; CH_2), 0.85–0.71 (m, 16H; Me/CH_2), 0.61–0.42 ppm (m, 4H; CH_2); ^{13}C NMR (75 MHz, $CDCl_3$): δ=193.3 (C), 158.7 (C), 156.4 (C), 151.6 (C), 151.1 (C), 150.4 (C), 148.4 (C), 147.5 (C), 144.6 (C), 144.0 (C), 143.0 (C), 142.6 (C), 142.0 (C), 141.1 (C), 140.5 (C), 140.0 (C), 139.8 (C), 135.4 (C), 134.3 (C), 133.1 (CH), 131.3 (CH), 129.4 (CH), 128.7 (CH), 128.14 (CH), 128.06 (CH), 127.9 (CH), 127.6 (CH), 127.3 (CH), 124.4 (CH), 122.6 (CH), 120.2 (CH), 116.0 (CH), 115.7 (CH), 115.5 (CH), 115.2 (CH), 115.1 (CH), 114.5 (CH), 66.0 (C), 55.6 (C), 54.8 (C), 40.5 (CH_2), 40.3 (CH_2), 31.8 (CH_2), 31.7 (CH_2), 30.0 (CH_2), 29.9 (CH_2), 29.7 (CH_2), 29.18 (CH_2), 29.15 (CH_2), 29.1 (CH_2), 23.8 (CH_2), 23.7 (CH_2), 22.6 (CH_2), 22.5 (CH_2), 14.1 (Me), 14.0 ppm (Me); IR (KBr): $\tilde{\nu}$= 3060, 2923, 2852, 1714 (C=O), 1597, 1419, 1283 cm^{-1}; UV/Vis (CH_2Cl_2): λ_{max}=385 (ε=21419), 365 (14851), 322 (13367), 309 nm (12889 $M^{-1}cm^{-1}$); HRMS (ESI): *m/z*: calcd for $C_{78}H_{90}O$+Na: 1065.68894 $[M+Na]^+$; found: 1065.6883.

6,15-Dibiphenyl-2-yl-9,9,18,18-tetraoctyl-6,9,15,18-tetrahydrobenzo[5,6]-*s*-indaceno[1,2-*b*]indeno[2,1-*h*]fluorene-6,15-diol (11)

Route 1: 2-Bromobiphenyl (1.85 g, 1.37 mL, 7.93 mmol) was dissolved in dry THF (60 mL) in a Schlenk tube under an argon atmosphere and the solution was degassed and cooled to −78 °C. *n*BuLi (1.6 M in hexane, 5.46 mL, 8.73 mmol) was added dropwise over 45 min. The resulting yellow solution was stirred for a further 45 min and **10** (0.80 g, 0.88 mmol) dissolved in dry, degassed and cooled (−78 °C) THF was added dropwise through a cannula. The reaction was stirred overnight (from −78 °C to room temperature) and the resulting mixture was poured into a saturated solution of ammonium chloride (40 mL) and extracted with CH_2Cl_2 (5×20 mL). The extracts were dried ($MgSO_4$), the solvent was removed in vacuo and the residue was purified by column chromatography on silica gel eluting with CH_2Cl_2/light petroleum (1:2) to give **11** as a red solid (0.34 g, 31%).

Route 2: *D*iketone **10** (100 mg, 0.11 mmol) was dissolved in dry and degassed THF (10 mL) in a Schlenk tube under an argon atmosphere. A solution of biphenyl-2-ylmagnesium bromide (0.5 M in diethyl ether, 2.1 mL, 0.99 mmol) was added. The reaction was stirred overnight at room temperature and the resulting mixture was poured into a saturated solution of ammonium chloride (10 mL) and extracted with CH_2Cl_2 (5×10 mL). The extracts were dried ($MgSO_4$), the solvent was removed in vacuo and the residue was purified by column chromatography on silica gel eluting with CH_2Cl_2/light petroleum (1:2) to give **11** as a red solid (29 mg, 22%). M.p. 171 °C; ^{1}H NMR (300 MHz, $CDCl_3$): δ=8.64 (d, J=7.5 Hz, 2H; ArH), 7.69–7.61 (m, 4H; ArH), 7.53 (s, 2H; ArH), 7.40 (t, J=7.5 Hz, 2H; ArH), 7.34–7.28 (m, 6H; ArH), 7.12 (s, 2H; ArH), 7.00 (s, 2H; ArH), 6.94 (d, J=7.5 Hz, 2H; ArH), 6.83 (t, J=7.5 Hz, 2H; ArH), 6.62 (br m, 2H; ArH), 6.51 (br m, 2H; ArH), 6.20 (br m, 2H; ArH), 6.02 (br m, 2H; ArH), 2.32 (s, 2H; exch D_2O, OH), 1.95 (t, J=7.2 Hz, 8H; CH_2), 1.30–1.08 (m, 40H; CH_2), 0.81 (t, J=7.2 Hz, 12H; Me), 0.73–0.54 ppm (m, 8H; CH_2); ^{13}C NMR (75 MHz, $CDCl_3$): δ=52.3 (C), 151.9 (C), 151.0 (C), 150.0 (C), 141.2 (C), 141.0 (C), 140.7 (C), 140.6 (C), 140.4 (C), 139.9 (C), 139.3 (C), 131.5 (CH), 129.0 (CH), 127.3 (CH), 127.0 (CH), 126.9 (CH), 126.7 (CH), 126.5 (CH), 125.4 (CH), 122.8 (CH), 122.7 (CH), 119.7 (CH), 115.8 (CH), 115.7 (CH), 114.6 (CH), 81.7 (COH), 54.8 (C), 40.7 (CH_2), 31.7 (CH_2), 30.3 (CH_2), 30.0 (CH_2), 29.2 (CH_2), 23.8 (CH_2), 22.6 (CH_2), 14.0 ppm (Me); IR (KBr): $\tilde{\nu}$=3056, 2925, 2852, 1583, 1477, 1435, 1418, 1271, 1180 cm^{-1}; HRMS (ESI): *m/z*: calcd for $C_{90}H_{102}O_2$+Na: 1237.77775 $[M+Na]^+$; found: 1237.7775.

9′,9′,18′,18′-Tetraoctyl-9′,18′-dihydrodispiro[fluorene-9,6′-benzo[5,6]-*s*-indaceno[1,2-*b*]indeno[2,1-*h*]fluorene-15′,9″-fluorene] (2): Diol **11** (342 mg, 0.28 mmol) was dissolved in CH_2Cl_2 (100 mL) and a solution of boron trifluoride diethyl etherate (145 μL, 166 mg, 1.12 mmol) was added. The solution was stirred at room temperature for 10 min. The solvent was evaporated in vacuo. The residue was purified by column chromatography on silica gel eluting with CH_2Cl_2/light petroleum (1:2) to give **2** as a colorless solid (210 mg, 64%). M.p. 246 °C (CH_2Cl_2/acetonitrile); ^{1}H NMR (300 MHz, CD_2Cl_2): δ=8.01 (d, J=7.5 Hz, 4H; ArH), 7.56 (s, 2H; ArH), 7.48 (t, J=7.5 Hz, 4H; ArH), 7.35 (d, J=7.5 Hz, 2H; ArH), 7.28–7.12 (m, 12H; ArH), 6.98 (s, 2H; ArH), 6.88 (d, J=7.5 Hz, 4H; ArH), 1.93 (t, J=7.2 Hz, 8H; CH_2), 1.27–1.00 (m, 40H; CH_2), 0.79 (t, J=7.2 Hz, 12H; Me), 0.65–0.40 ppm (m, 8H; CH_2); ^{13}C NMR (75 MHz, $CDCl_3$): δ=151.0 (C), 150.8 (C), 149.6 (C), 149.1 (C), 147.8 (C), 141.9 (C), 141.8 (C), 141.0 (C), 140.9 (C), 140.8 (C), 127.9 (CH), 127.7 (CH), 126.6 (CH), 126.4 (CH), 124.4 (CH), 122.6 (CH), 120.1 (CH), 119.6 (CH), 115.2 (CH), 115.0 (CH), 114.4 (CH), 65.6 (C), 54.7 (C), 40.6 (CH_2), 31.7 (CH_2), 30.0 (CH_2), 29.7 (CH_2), 29.2 (CH_2), 23.7 (CH_2), 22.6 (CH_2), 14.0 ppm (Me); IR (KBr): $\tilde{\nu}$=3059, 2924, 2850, 1461, 1373, 1267 cm^{-1}; UV/Vis (CH_2Cl_2): λ_{max}=394 (ε=97366), 373 (64400), 339 nm (18806 $M^{-1}cm^{-1}$); HRMS (LSIMS): *m/z*: calcd for $C_{90}H_{98}$: 1178.76685 $[M]^+$; found: 1178.7662; elemental analysis calcd (%) for $C_{90}H_{98}$: C 91.63, H 8.37; found: C 91.13, H 8.57.

Spectroscopic studies: Cyclohexane (ACS grade) and toluene (semiconductor grade) were purchased from Alfa Aesar. Oligomers **1** and **2** (15 mg mL^{-1} in toluene, 90 μL) were deposited on quartz substrate by using a home-made spin-coater and the UV/Vis and photoluminescence spectra were immediately recorded. UV/Vis spectra of the thin films were recorded by using a UV/Vis SHIMADZU UV-1605 spectrophotometer. UV/Vis spectra of solutions were recorded by using either a UV/Vis/NIR CARY 5000-Varian (for quantum yield determination) or a UV/Vis UVIKON XL Biotech spectrophotometer. The optical band gap was calculated from the absorption edge of the UV/Vis absorption spectra by using the formula ΔE^{opt} [eV]=$hc\lambda^{-1}$, in which λ is the absorption edge (in metres). With $h=6.626\times10^{-34}$ J s (1 eV=1.602×10^{-19} J) and $c=2.997\times10^{8}$ m s^{-1}. Photoluminescence spectra of the solutions (cyclohexane) or thin films were recorded with a PTI spectrofluorimeter (PTI-814 PDS, MD 5020, LPS 220B) by using a xenon lamp. Quantum yields in solution (ϕ_{sol}) were calculated relative to quinine sulfate (ϕ_{sol}=0.546 in 1 N H_2SO_4) using standard procedures.[41] ϕ_{sol} was determined according to Equation (1), in which subscripts s and r refer to the sample and the reference, respectively. The integrated area of the emission peak in arbitrary units is given as *T*, *n* is the refracting index of the solvent (n_s=1.42662 for cyclohexane) and *A* is the absorbance. IR spectra were recorded on a BIORAD IRFTS175C spectrometer.

$$\phi_{sol} = 100\phi_{ref}\frac{(T_sA_r)}{(T_rA_s)}\left[\frac{n_s}{n_r}\right]^2 \quad (1)$$

Thermal analysis: Thermogravimetric analyses (TGA) were carried out with a Rigaku Thermoflex instrument under a nitrogen atmosphere between room temperature and 1000 °C at a heating rate of 5 °C min^{-1}. Melting points were determined by using an Electrothermal® melting point apparatus.

Electrochemical studies: All electrochemical experiments were performed under an argon atmosphere using a platinum disk electrode (diameter 1 mm). The counter electrode was a vitreous carbon rod and the reference electrode was a silver wire in a 0.1 M solution of $AgNO_3$ in

CH_3CN. Ferrocene was added to the electrolyte solution at the end of a series of experiments. The ferrocene/ferrocenium (Fc/Fc^+) couple served as internal standard. The three-electrode cell was connected to a PAR Model 173 potentiostat monitored with a PAR Model 175 signal generator and a PAR Model 179 signal coulometer. CV traces were recorded on an XY SEFRAM-type TGM 164 instrument. Acetonitrile with less than 5‰ of water (ref. SDS 00610S21) and CH_2Cl_2 with less than 100 ppm of water (ref. SDS 02910E21) were used without purification. Activated Al_2O_3 was added to the electrolytic solution to remove excess moisture. For further comparison of the electrochemical and optical properties, all potentials are referred to the SCE electrode, which was calibrated at −0.405 V versus Fc/Fc^+. Following the work of Jenekhe and co-workers,[57] we estimated the electron affinity (EA), or LUMO, and the ionisation potential (IP), or HOMO, from the redox data. The LUMO level was calculated from LUMO [eV] $= -[E_{red}^{onset}$ (vs. SCE)+4.4] and the HOMO level from HOMO [eV] $= -[E_{ox}^{onset}$ (vs. SCE)+4.4], based on an SCE energy level of 4.4 eV relative to the vacuum. The electrochemical gap was calculated from $\Delta E^{El} = |\text{HOMO} - \text{LUMO}|$ (in eV).

Computational details: Calculations were performed on a simplified model of **2** in which the octyl chains were omitted and replaced by methyl groups. Full geometry optimisation by DFT[74,75] calculations were performed with the hybrid Becke-3 parameter exchange functional [60,76,77] and the Lee–Yang–Parr non-local correlation functional[78] (B3LYP or UB3LYP) implemented in the Gaussian 03 (Revision D.02) suite of programs[56] using the 6-31G* basis set[79] and the default convergence criterion implemented in the program. The figures were generated with MOLEKEL 4.3.[59]

X-Ray determination: Data were collected by using a Rigaku MM007 RA/confocal optics generator and Saturn70 CCD diffractometer. In both **2** and **8** the crystal quality/diffraction was poor and several different crystals were examined with consistent results. The structures were solved by direct methods and refined by full-matrix least-squares on F^2 values of all data.[80]

Oligomer **2**: $C_{98}H_{115}$; $M = 1292.90$; yellow platelet; crystal size $0.35 \times 0.08 \times 0.01$ mm; triclinic; $P\bar{1}$; $a = 12.676(7)$, $b = 13.014(8)$, $c = 13.240(7)$ Å; $\alpha = 84.53(5)$, $\beta = 76.25(4)$, $\gamma = 83.29(5)°$; $V = 2101.9(19)$ Å^3; $Z = 1$; $\rho_{calcd} = 1.021$ Mg m^{-3}; $Mo_{K\alpha}$ radiation (confocal optic, $\lambda = 0.71073$ Å); $\mu = 0.057$ mm^{-1}; $T = 93(2)$ K; 15920 data (6963 unique, $R_{int} = 0.0792$, $2.030 < \theta < 25.42°$); $wR = \{\Sigma[w(F_o^2 - F_c^2)^2]/\Sigma[w(F_o^2)^2]\}^{1/2} = 0.3413$; conventional $R = 0.1218$ for F values of reflections with $F_o^2 > 2\sigma(F_o^2)$ (4932 observed reflections); $S = 1.082$ for 480 parameters. Residual electron density extremes were 0.547 and −0.299 e Å^{-3}.

Compound **8**: $C_{70}H_{94}O_4$; $M = 999.45$; colorless platelet; crystal size $0.1 \times 0.1 \times 0.01$ mm; triclinic; $P\bar{1}$; $a = 8.963(3)$, $b = 18.085(6)$, $c = 19.344(6)$ Å; $\alpha = 97.389(6)$, $\beta = 100.353(5)$, $\gamma = 94.091(5)°$; $V = 3044.6(17)$ Å^3; $Z = 2$; $\rho_{calcd} = 1.090$ Mg m^{-3}; $Mo_{K\alpha}$ radiation (confocal optic, $\lambda = 0.71073$ Å); $\mu = 0.065$ mm^{-1}; $T = 93(2)$ K; 30488 data (11031 unique, $R_{int} = 0.0887$, $2.16 < \theta < 25.36°$); $wR = \{\Sigma[w(F_o^2 - F_c^2)^2]/\Sigma[w(F_o^2)^2]\}^{1/2} = 0.1838$; conventional $R = 0.0958$ for F values of reflections with $F_o^2 > 2\sigma(F_o^2)$ (7989 observed reflections); $S = 1.053$ for 669 parameters. Residual electron density extremes were 0.506 and −0.268 e Å^{-3}.

CCDC-689480 and 689481 contain the supplementary crystallographic data for this paper. These data can be obtained free of charge from The Cambridge Crystallographic Data Centre via www.ccdc.cam.ac.uk/data_request/cif

EL fabrication and testing: OLEDs were fabricated by using the following procedure. Indium–tin oxide (ITO) substrates on glass from Merck were submitted to solvent ultrasonic cleansing with acetone and isopropanol followed by UV/ozone treatment for 20 min. A layer of poly(3,4-ethylenedioxythiophene) doped with poly(styrene sulfonate) (PEDOT/PSS from HC Starck) was then deposited onto the ITO by spin-coating at 4000 rpm from a 3 wt% water dispersion to form a layer 40 nm thick. This layer improves hole injection from the ITO to the HOMO level of the organic material and increases the performances and the lifetime of the device.[81] PEDOT/PSS was subsequently annealed at 80 °C under vacuum for 30 min. Then the emissive layer was either spin-coated or thermally evaporated. The spin-coating was carried out at 1000 rpm from a 20 mg mL^{-1} solution in cyclohexanone. The evaporation was performed under vacuum (ca. 10^{-6} mbar) at a low deposition rate of 0.1 nm s^{-1}. The layer thickness was monitored in situ by a piezoelectric quartz balance during the evaporation. Calcium cathodes were finally evaporated through a shadow mask. The OLEDs were then stored and characterised under an inert atmosphere in a nitrogen glove box. Current–voltage–luminance (I–V–L) curves were recorded by using a Keithley 4200 SCS instrument. Light emission was collected by using a calibrated photodiode coupled to a Hamamatsu Photosensor amplifier C9329. Electroluminescence spectra were measured with a CCD spectrometer (Ocean Optics HR 2000). The microscope images were taken with a Zeiss Axio Imager A1/F1 coupled to a digital camera using a ×20 lens.

Acknowledgements

N.C. thanks le ministère de l'éducation nationale, de la recherche et de la technologie (MENRT) for a studentship. The authors would like to thank the CINES (Centre Informatique National de l'Enseignement Supérieur, Montpellier) for awarding computing time, the CRMPO (Centre Régional de Mesure Physique de l'Ouest) for high-resolution mass measurements and CHN analyses. Prof. Muriel Hissler and Dr. Olivier Jeannin are strongly acknowledged for helpful discussions in thin-film fluorescence studies and in X-ray diffraction, respectively. We also thank Damien Thirion, Ali Yassin, Sébastien Bivaud and Stephanie Fryars for invaluable technical assistance.

[1] K. Müllen, U. Scherf, *Organic Light-Emitting Devices: Synthesis Properties and Applications*, Wiley-VCH, Weinheim, **2006**.
[2] A. C. Grimsdale, K. Müllen, *Macromol. Rapid Commun.* **2007**, *28*, 1676–1702.
[3] U. Scherf, *J. Mater. Chem.* **1999**, *9*, 1853–1864.
[4] V. N. Bliznyuk, S. A. Carter, J. C. Scott, G. Klärner, R. D. Miller, D. C. Miller, *Macromolecules* **1999**, *32*, 361–369.
[5] J.-I. Lee, G. Klaerner, R. D. Miller, *Chem. Mater.* **1999**, *11*, 1083–1086.
[6] L. Romaner, A. Pogantsch, P. Scandiucci de Freitas, U. Scherf, M. Gaal, E. Zojer, E. J. W. List, *Adv. Funct. Mater.* **2003**, *13*, 597–601.
[7] M. Gaal, E. J. W. List, U. Scherf, *Macromolecules* **2003**, *36*, 4236–4237.
[8] T. P. I. Saragi, T. Spehr, A. Siebert, T. Fuhrmann-Lieker, J. Salbeck, *Chem. Rev.* **2007**, *107*, 1011–1065.
[9] R. Pudzich, T. Fuhrmann-Lieker, J. Salbeck, *Adv. Polym. Sci.* **2006**, *199*, 83–142.
[10] R. Wu, J. S. Schumm, D. L. Pearson, J. M. Tour, *J. Org. Chem.* **1996**, *61*, 6906–6921.
[11] J. M. Tour, R. Wu, J. S. Schumm, *J. Am. Chem. Soc.* **1991**, *113*, 7064–7066.
[12] J. M. Tour, R. Wu, J. S. Schumm, *J. Am. Chem. Soc.* **1990**, *112*, 5662–5663.
[13] J. Guay, A. Diaz, R. Wu, J. M. Tour, *J. Am. Chem. Soc.* **1993**, *115*, 1869–1874.
[14] N. Johansson, D. A. Dos Santos, S. Guo, J. Cornil, M. Fahlman, J. Salbeck, H. Schenk, H. Arwin, J.-L. Bredas, W. R. Salaneck, *J. Chem. Phys.* **1997**, *107*, 2542–2549.
[15] N. Johansson, J. Salbeck, J. Bauer, F. Weissörtel, P. Bröms, A. Andersson, W. R. Salaneck, *Adv. Mater.* **1998**, *10*, 1136–1141.
[16] R. Pudzich, J. Salbeck, *Synth. Met.* **2003**, *138*, 21–31.
[17] J. Salbeck, F. Weissörtel, J. Bauer, *Macromol. Symp.* **1997**, *125*, 121–132.
[18] J. Salbeck, N. Yu, J. Bauer, F. Weissörtel, H. Besten, *Synth. Met.* **1997**, *91*, 209–215.
[19] T. Spehr, R. Pudzich, P. Fuhrmann, J. Salbeck, *Org. Electron.* **2003**, *4*, 61–69.
[20] U. Scherf, K. Müllen, *Macromolecules* **1992**, *25*, 3546–3548.
[21] J. Jacob, S. Sax, T. Piok, E. J. W. List, A. C. Grimsdale, K. Müllen, *J. Am. Chem. Soc.* **2004**, *126*, 6987–6995.

[22] J. Jacob, S. Sax, M. Gaal, E. J. W. List, A. C. Grimsdale, K. Müllen, *Macromolecules* **2005**, *38*, 9933–9938.
[23] F. Schindler, J. Jacob, A. C. Grimsdale, U. Scherf, K. Müllen, J. M. Lupton, J. Feldmann, *Angew. Chem.* **2005**, *117*, 1544–1549; *Angew. Chem. Int. Ed.* **2005**, *44*, 1520–1525.
[24] A. K. Mishra, M. Graf, F. Grasse, J. Jacob, E. J. W. List, K. Müllen, *Chem. Mater.* **2006**, *18*, 2879–2885.
[25] G. Zhou, M. Baumgarten, K. Müllen, *J. Am. Chem. Soc.* **2007**, *129*, 12211–12221.
[26] Y. Wu, J. Zhang, Z. Bo, *Org. Lett.* **2007**, *9*, 4435–4438.
[27] D. Vak, B. Lim, S.-H. Lee, D.-Y. Kim, *Org. Lett.* **2005**, *7*, 4229–4232.
[28] D. Horhant, J.-J. Liang, M. Virboul, C. Poriel, G. Alcaraz, Rault- J. Berthelot, *Org. Lett.* **2006**, *8*, 257–260.
[29] C. Poriel, J.-J. Liang, J. Rault-Berthelot, F. Barrière, N. Cocherel, A. M. Z. Slawin, D. Horhant, M. Virboul, G. Alcaraz, N. Audebrand, L. Vignau, N. Huby, L. Hirsch, G. Wantz, *Chem. Eur. J.* **2007**, *13*, 10055–10069.
[30] C. Poriel, J. Rault-Berthelot, F. Barrière, A. M. Z. Slawin, *Org. Lett.* **2008**, *10*, 373–376.
[31] M. Kimura, S. Kuwano, Y. Sawaki, H. Fujikawa, K. Noda, Y. Taga, K. Takagi, *J. Mater. Chem.* **2005**, *15*, 2393–2398.
[32] L.-H. Xie, X.-Y. Hou, C. Tang, Y.-R. Hua, R.-J. Wang, R.-F. Chen, Q.-L. Fan, L.-H. Wang, W. Wei, B. Peng, W. Huang, *Org. Lett.* **2006**, *8*, 1363–1366.
[33] L. Oldridge, M. Kastler, K. Müllen, *Chem. Commun.* **2006**, 885–887.
[34] F. Uckert, S. Setayesh, K. Müllen, *Macromolecules* **1999**, *32*, 4519–4524.
[35] T. Nakagawa, D. Kumaki, J.-I. Nishida, S. TOkito, Y. Yamashita, *Chem. Mater.* **2008**, *20*, 2615–2617.
[36] H. Usta, A. Facchetti, T. J. Marks, *Org. Lett.* **2008**, *10*, 1385–1388.
[37] R. G. Clarkson, M. Gomberg, *J. Am. Chem. Soc.* **1930**, *52*, 2881–2891.
[38] J. H. Weisburger, E. K. Weisburger, F. E. Ray, *J. Am. Chem. Soc.* **1950**, *72*, 4250–4253.
[39] J. H. Weisburger, E. K. Weisburger, F. E. Ray, *J. Am. Chem. Soc.* **1950**, *72*, 4253–4255.
[40] B. Winter-Werner, F. Diederich, V. Gramlich, *Helv. Chim. Acta* **1996**, *79*, 1338–1360.
[41] S. Merlet, M. Birau, Z. Y. Wang, *Org. Lett.* **2002**, *4*, 2157–2159.
[42] C. Poriel, Y. Ferrand, S. Juillard, P. Le Maux, G. Simonneaux, *Tetrahedron* **2004**, *60*, 145–158.
[43] Our previously reported approach to **1** led to an overall yield of around 20%.[29]
[44] M. Sonntag, K. Kreger, D. Hanft, P. Strohriegl, S. Setayesh, D. de Leeuw, *Chem. Mater.* **2005**, *17*, 3031–3039.
[45] M. Belletête, S. Beaupré, J. Bouchard, P. Blondin, M. Leclerc, G. Durocher, *J. Phys. Chem. B* **2000**, *104*, 9118–9125.
[46] T. Li, T. Yamamoto, H.-L. Lan, J. Kido, *Polym. Adv. Technol.* **2004**, *15*, 266–269.
[47] J. J. S. Lamba, J. M. Tour, *J. Am. Chem. Soc.* **1994**, *116*, 11723–11736.
[48] R. Laufer, G. I. Dmitrienko, *J. Am. Chem. Soc.* **2002**, *124*, 1854–1855.
[49] H. Koyama, T. Kamikawa, *J. Chem. Soc. Perkin Trans. 1* **1998**, 203–209.
[50] Note that several other groups have also reported low-to-moderate yields for similar coupling reactions, see references. [27], [31] and [52].
[51] When the cyclisation was performed by heating at reflux in AcOH/HCl, we always observed the presence of an impurity with a strong yellow emission under a UV lamp (365 nm), which, despite several attempts, could not be separated from **2**.
[52] J. Luo, Y. Zhou, Z.-Q. Niu, Q.-F. Zhou, Y. Ma, J. Pei, *J. Am. Chem. Soc.* **2007**, *129*, 11314–11315.
[53] K.-T. Wong, L.-C. Chi, S.-C. Huang, Y.-L. Liao, Y.-H. Liu, Y. Wang, *Org. Lett.* **2006**, *8*, 5029–5032.
[54] M. Zhang, C. Yang, A. K. Mishra, W. Pisula, G. Zhou, B. Schmaltz, M. Baumgarten, K. Müllen, *Chem. Commun.* **2007**, 1704–1706.
[55] In the simplified model of **2**, octyl chains have been replaced by methyl groups.
[56] Gaussian 03, Revision D.02, M. J. Frisch, G. W. Trucks, H. B. Schlegel, G. E. Scuseria, M. A. Robb, J. R. Cheeseman, J. A. Montgomery, Jr., T. Vreven, K. N. Kudin, J. C. Burant, J. M. Millam, S. S. Lyengar, J. Tomasi, V. Barone, B. Mennucci, M. Cossi, G. Scalmani, N. Rega, G. A. Petersson, H. Nakatsuji, M. Hada, M. Ehara, K. Toyota, R. Fukuda, J. Hasegawa, M. Ishida, T. Nakajima, Y. Honda, O. Kitao, H. Nakai, M. Klene, X. Li, J. E. Knox, H. P. Hratchian, J. B. Cross, C. Adamo, J. Jaramillo, R. Gomperts, R. E. Stratmann, O. C. Yazyev, A. J. Austin, R. Cammi, C. Pomelli, J. W. Ochterski, P. Y. Ayala, K. Morokuma, G. A. Voth, P. Salvador, J. J. Dannenberg, V. G. Zakrzewski, S. Dapprich, A. D. Daniels, M. C. Strain, O. Farkas, D. K. Malick, A. D. Rabuck, K. Raghavachari, J. B. Foresman, J. V. Ortiz, Q. Cui, A. G. Baboul, S. Clifford, J. Cioslowski, B. Stefanov, G. Liu, A. Liashenko, P. Piskorz, I. Komaromi, R. L. Martin, D. J. Fox, T. Keith, M. A. Al-Laham, C. Y. Peng, A. Nanayakkara, M. Challacombe, P. M. W. Gill, B. Johnson, W. Chen, M. W. Wong, C. Gonzalez, J. A. Pople, Gaussian, Inc., Wallingford, CT, **2004**.
[57] A. P. Kulkarni, C. J. Tonzola, A. Babel, S. A. Jenekhe, *Chem. Mater.* **2004**, *16*, 4556–4573.
[58] Y. Zhu, R. D. Champio, S. A. Jenekhe, *Macromolecules* **2006**, *39*, 8712–8719.
[59] MOLEKEL 4.3, H. P. Flükiger, S. Lüthi, S. Portmann, J. Weber, Swiss National Supercomputing Centre CSCS, Manno (Switzerland), **2000**.
[60] A. D. Becke, *J. Chem. Phys.* **1993**, *98*, 5648–5652.
[61] C. Zhao, Y. Zhang, M.-K. Ng, *J. Org. Chem.* **2007**, *72*, 6364–6371.
[62] J. Rault-Berthelot, C. Poriel, F. Justaud, F. Barrière, *New J. Chem.* **2008**, *32*, 1259–1266.
[63] A. Kuboyama, *Bull. Chem. Soc. Japan* **1964**, *37*, 1540–1544.
[64] F. Jaramillo-Isaza, M. L. Turner, *J. Mater. Chem.* **2006**, *16*, 83–89.
[65] Optical band gap estimated from the low-energy edge of the UV/Vis spectrum in CH_2Cl_2.
[66] M. Belletête, M. Ranger, S. Beaupré, M. Leclerc, G. Durocher, *Chem. Phys. Lett.* **2000**, *316*, 101–107.
[67] F.-I. Wu, R. Dodda, D. Sahadeva Reddy, C.-F. Shu, *J. Mater. Chem.* **2002**, *12*, 2893–2897.
[68] F. Le Floch, Ph.D. Thesis, University of Rennes I (France), **2003**.
[69] K.-T. Wong, Y.-Y. Chien, R.-T. Chen, C.-F. Wang, Y.-T. Lin, H.-H. Chiang, P.-Y. Hsieh, C.-C. Wu, C.-H. Chou, Y. O. Su, G.-H. Lee, S.-M. Peng, *J. Am. Chem. Soc.* **2002**, *124*, 11576–11577.
[70] M. M. Elmahdy, G. Floudas, L. Oldridge, A. C. Grimsdale, K. Müllen, *ChemPhysChem* **2006**, *7*, 1431–1441.
[71] H. Etori, X. L. Jin, T. Yasuda, S. Mataka, T. Tsutsui, *Synth. Met.* **2006**, *156*, 1090–1096.
[72] J. Jacob, J. Zhang, A. C. Grimsdale, K. Müllen, M. Gaal, E. J. W. List, *Macromolecules* **2003**, *36*, 8240–8245.
[73] L. Romaner, G. Heimel, H. Wiesenhofer, P. Scandiucci de Freitas, U. Scherf, J. L. Brédas, E. Zojer, E. J. W. List, *Chem. Mater.* **2004**, *16*, 4667–4674.
[74] P. Hohenberg, W. Kohn, *Phys. Rev.* **1964**, *136*, B864–B871.
[75] R. G. Parr, W. Yang, *Density-Functional Theory of Atoms and Molecules*, Oxford University, Oxford, **1989**.
[76] A. D. Becke, *Phys. Rev.* **1988**, *38*, 3098–3100.
[77] A. D. Becke, *J. Chem. Phys.* **1993**, *98*, 1372–1377.
[78] C. Lee, W. Yang, R. G. Parr, *Phys. Rev. B* **1988**, *37*, 785–789.
[79] P. C. Hariharan, J. A. Pople, *Chem. Phys. Lett.* **1972**, *16*, 217–219.
[80] SHELXTL, version 6.1, G. M. Sheldrick, Bruker AXS, Madison, WI, **2001**
[81] A. van Dijken, A. Perro, E. A. Meulenkamp, K. Brunner, *Org. Elec.* **2003**, *4*, 131–141.

Received: July 15, 2008
Published online: November 13, 2008

